December 22, 1999
FINAL REPORT

BAY BRIDGE DOWNHOLE ARRAY ANALYSES

Prepared for

Earth Mechanics Inc
17660 Newhope Street, Suite E
Fountain Valley, CA 92708

by

Bob Darragh
Walt Silva
Nick Gregor

of

Pacific Engineering and Analysis
311 Pomona Avenue
El Cerrito, CA 94530

CONTENTS

LIST OF TABLES

LIST OF FIGURES

LIST OF FIGURES

LIST OF FIGURES

LIST OF FIGURES
APPENDIX A

1.0 INTRODUCTION

Vertical ground motion array data were collected and analyzed to support recommendations for the design of the San Francisco - Oakland Bay Bridge. The areas of design concern and investigation are the V/H (vertical/horizontal) response spectral ratio as a function of magnitude, source distances (epicentral and focal), peak ground acceleration level, and the vertical wave propagation velocity as a function of frequency. The properties of recorded vertical and horizontal ground motions that affect these design concerns are evaluated as a function of sensor depth in the vertical arrays.

2.0 VERTICAL ARRAY DATA COLLECTION

Ground motion data were collected from ten vertical ground motion arrays (Table 1) located California, Japan, and Taiwan. At each array, three components of ground acceleration are recorded at or near the surface and at various depths. The deepest sensor depths of 252 and 220 m are recorded at the La Cienega and Garner Valley arrays, respectively (Table 1). In contrast, the shallowest sensor depths, ranging from 5 to 8 m, are recorded by the CHIBA, Garner Valley, LSST-Lotung, Treasure Island, and Wildlife Liquefaction arrays. The Treasure Island array, recording twenty-one acceleration time histories from sensors located at the surface and six depths, is the densest vertical array (Darragh and others, 1993). Table 1 lists the arrays, sensor depths, and events analyzed.

Earthquake magnitude ranges from 2.3 to 7.8 with epicentral distances extending from 1 to 177 km. The focal depths for shallow earthquakes located in the crust ranges from 2 to 20 km. For intermediate earthquakes located below the crust the depth range is from 48 to 96 km. These deep earthquakes were recorded at the CHIBA array, Japan. Measured P-wave and S-wave velocity profiles for the ten arrays are shown in Appendix A.

Peak vertical or horizontal accelerations larger than 0.1 g were recorded at six arrays (Kainan, LSST-Lotung (4 earthquakes), Port Island, Takasago, Techcent, and Wildlife Liquefaction (2 earthquakes)). The largest peak vertical acceleration of 0.84 g was recorded at the Port Island array at a depth of 16 m during the 1995 Kobe mainshock. The largest peak vertical acceleration recorded in California of 0.43 g was recorded at the Wildlife Liquefaction array.

Additional data were collected from the following arrays: Anza, EPRI Parkfield, Richmond Field Station, McGee Creek, and San Francisco Marina in California and Ashigara Valley in Japan. Data from these arrays are not included in the analyses due to either very small levels of motion, velocity rather than acceleration time history recordings, or constraints in time.

3.0 CHARACTERISTICS OF SURFACE VERTICAL STRONG GROUND MOTIONS

Recent recordings in the near-source region ($D \leq 10$ to 15 km) of large earthquakes document characteristics of vertical strong ground motions that are appropriate for design and serve as a guide for the vertical array analyses in Section 4. For example, short period vertical motions can exceed horizontal motions (Niazi and Bozorgnia, 1991; Bozorgnia et al., 1995) at both rock and soil sites (EPRI, 1993). This section examines the dependencies of the surface

vertical-to-horizontal response spectral ratio (V/H) on magnitude, distance, and site conditions.

3.1 Short-period Time Domain

Figures 1 to 5 are accelation time history plots which illustrate general trends in short period vertical and horizontal motions. The intent is to show predominately SV-wave motion, for close fault distances ($\leq$ 10 to 15 km) on the vertical component with similar phasing as the horizontal components for rock sites while at soil sites, P-waves dominate the vertical motions showing earlier arriving and larger higher frequency energy content. At more distant sites, P-wave energy tends to be dominant on the vertical component at both rock and soil sites. These trends may be complicated by P-wave and S-wave radiation patterns, near surface amplification, and topographic effects.

To illustrate these effects on acceleration time histories for vertical and horizontal components, a series of plots from the California Division of Mines and Geology Strong Motion Instrumentation Program earthquake data quick reports are presented. These plots show all three components for each site in a convenient format for illustrative purposes.

To consider first close-in rock sites, Figure 1 shows three component acceleration time histories at the Pacoima Dam (Downstream) and Corralitos sites for the 1994 **M** 6.7 Northridge and 1989 **M** 6.9 Loma Prieta earthquakes. Both sites are within about an 8 km fault distance and both sets of records show very similar motions on the horizontal and vertical components. Structures founded on rock conditions at close distances may then be expected to experience simultaneous horizontal and vertical demands at similar levels and over a fairly broad period range.

For close-in soil sites, Figure 2 shows distinctly different features in the Sylmar County Hospital and Arleta records for the Northridge earthquake. As for the rock sites, the soil sites are close-in recordings at fault distances of 6.1 km for Sylmar and 9.2 km for Arleta. Unlike the rock site recordings however, the soil site records show strong short-period motion arriving significantly before the large horizontal motions. Structures founded on deep soil would then be expected to experience vertical and horizontal demands significantly different than on rock conditions. The vertical demands at close-in soil sites would generally be characterized as out of phase with the dominant horizontal motions and of much shorter periods. The largest short period motions on the vertical component may arrive before those of the horizontal and will be larger than the short period horizontal motions. During the passage of the dominant horizontal component motions, the vertical demands on a structure could be characterized as random high-frequency chatter which may exceed 1 g at short periods. This is markedly different than the vertical motions at close-in rock sites, which tend to show strong low frequency coherence with the horizontal motions.

For the more distant sites, Figure 3 shows some interesting features across the Gilroy array for motions due to the 1989 Loma Prieta earthquake. Rock sites Gilroy #6 and #7, at fault distances of 19.9 and 24.2 km respectively, show features similar to those at the close-in soil site: earlier arriving and high-frequency vertical motions out-of-phase with the dominant horizontal motions. At rock site Gilroy #1 however, at a fault distance of 11.2 km, the vertical motions

display early arriving high frequency energy as well as low-frequency energy coherent with the dominant horizontal motions. A possible explanation for this behavior is that this site, at a fault distance of about 11 km, is in the transition region from close-in to more distant rock site characteristics.

An interesting and apparent contradiction to the expected close-in rock site characteristics are the recordings at Pacoima Kagel Canyon for the Northridge earthquake (Figure 4). This rock site is at a fault distance of 8.2 km, about the same distance as the Pacoima Downstream site (Figure 1), but displays soil site characteristics on the vertical component: early arriving high frequency energy and out-of-phase motions with the horizontal components. As part of a recent, Caltrans/NSF/EPRI sponsored project to Resolve Site Response Issues Associated with the Northridge Earthquake (ROSRINE), this recording site, as well as many others, has recently been drilled and logged. Based on the shear-wave velocity logging, the site is misclassified. With shear-wave velocities of just under 2,000 ft/sec from about 100 ft to the bottom of the hole at about 300 ft, the site is closer to a stiff soil than rock. This result is not entirely unexpected as the site is located in the Saugus formation, a typically soft Los Angeles area sandstone.

For the distant ($D \geq 10$ to 15 km) soil sites, Figure 5 shows the remaining sites across the Gilroy array which recorded the Loma Prieta earthquake. Site Gilroy #2 is at fault distance of 10.7 km and sites #3 and #4 are at fault distances of 14.4 and 16.1 km respectively. As with the close-in soil sites (Figure 2) and the distant rock sites (Figure 3), the vertical motions show high frequency early arriving energy and little coherence with the dominant horizontal motions.

3.2 Response Spectra

To examine distance and site condition dependencies of vertical motions in more detail, as well as broader period range, Figures 6 to 9 show 5% damped pseudo absolute response spectra for a selected set of sites. Cases examined are close-in and more distant rock and soil sites.

For the close-in rock site, Figure 6 shows response spectra computed for the vertical and two horizontal component records at the Southern California Edison Lucerne site from the 1992 **M** 7.2 Landers earthquake. The fault distance is about 2 km and the vertical component slightly exceeds the horizontal components at periods shorter than about 0.1 sec. At long periods, beyond about 1 sec, the vertical is comparable to the smaller of the horizontal components, the fault-parallel motion. The period range of nearly constant spectral acceleration in the horizontal components, about 2 to 5 sec, is likely due to the effects of directivity.

For the close-in soil site, Figure 7 show the response spectra at the Arleta site for the 1994 Northridge earthquake. The fault distance is 9.2 km and the vertical component greatly exceeds the horizontal components at periods shorter than about 0.2 sec. Beyond about 2 sec, as with the rock site Lucerne, the vertical component becomes comparable to the horizontal.

For the more distant sites, Figure 8 show response spectra for the Gilroy #6 rock site and Figure 9 show the corresponding plot for the Gilroy #4 soil site. The recordings are from the 1989 Loma Prieta earthquake at distances of 16.1 and 19.9 km for stations #4 and #6, respectively. For both sites, the short period vertical motions relative to the corresponding horizontal motions are

significantly reduced compared to the close-in sites. Interestingly, as with the close-in sites, the long period vertical motions approach the horizontal motions for periods beyond about 2 to 4 sec.

4.0 VERTICAL ARRAY DATA ANALYSES

The vertical array data analyses include examination of V/H response spectral ratios at 5% damping and several measurements of wave propagation velocity along (up) the vertical array. The data from the CHIBA, Japan array were excluded from some of the analyses since the recorded time histories are from deeper earthquakes with focal depths in excess of 48 km (Table 1). These deep earthquake sources do not reflect the crustal (shallow) earthquake sources in the vicinity of the San Francisco - Oakland Bay Bridge. The data from the Garner Valley array were also excluded from some of the analyses. High shear-wave velocities are present generally throughout the profile with weathered rock occurring at a depth of 19 to 25 m (Steidl and others, 1996). This site then represents an extremely stiff shallow soil site and is not considered representative of the soil sites along the San Francisco - Oakland Bay Bridge.

4.1 V/H Response Spectral Ratio (5% Damped)

The 5% damped response spectra are computed for the vertical and horizontal time histories. The average horizontal spectrum is the geometric mean of the two horizontal component spectra. The vertical spectrum divided by the average horizontal spectrum gives the V/H ratio. These ratios were studied as a function of sensor depth, peak ground acceleration, earthquake focal depth, and epicentral distance. All of the V/H ratios are normalized by the surface V/H ratio (Figures 10 to 13). Hence, on these Figures the normalized surface V/H ratio is a straight line at unity. Sensor depths are grouped into seven ranges to examine trends with depth. The ranges are: surface (0 to 1m), 5 to 9m, 10 to 19m, 20 to 39m, 40 to 55m, 83 to 122m, and 220 to 252m. Not all sensor depth ranges are represented on each Figure due to the selection criteria used. All Figures use triangular smoothing and are plotted as a function of period. Figures 10 to 13 exclude the Garner Valley array data, while Figure 12 also excludes the CHIBA array data.

The normalized V/H ratios in Figures 10 to 12 generally show at short periods (< 0.1 sec) that the surface V/H ratio is larger than the V/H ratios at depth. At long periods (> 1.0 sec) the surface V/H ratio is smaller than the V/H ratios at depth. The cross-over period where the surface V/H ratio is no longer larger than the V/H ratios at depth occurs generally between 0.1 to 1.0 sec. Also, V/H ratios tend to decrease with depth for periods less than the cross-over period (about 0.1 sec) and to increase with depth for periods greater than the cross-over period. Specifically, Figure 10 shows the normalized V/H ratio for all the data from the arrays in Table 1 excluding CHIBA and Garner Valley. Figures 11 and 12 investigate the ratio for parameters appropriate for the San Francisco - Oakland Bay Bridge, that is, magnitudes greater than 6, and peak horizontal acceleration at the surface greater than 0.1 g, respectively.

Also, these ratio trends are generally observed for the magnitudes ranges of less than 4, and between 4 and 5; focal depths less than 20 km; peak horizontal acceleration at the surface less than 0.1 g; and epicentral distance less than 15 km, and between 15 and 80 km. Exceptions do occur, for example for magnitudes between 5 and 6 (Figure 13) the normalized V/H ratio at depth is nearly always greater than unity. Also, for the CHIBA array with focal depths greater than 48 km

the V/H ratio at depth is larger than one at nearly all periods.

4.2 Uphole Velocity From Cross-Correlation Of Band-Pass Filtered Acceleration Time Histories

The cross-correlation as a function of time was calculated between two vertical time-histories located at different depths in a vertical array. The time-histories were band-pass filtered at 10 Hz and at 5 Hz using 5th order causal Butterworth filters with corner frequencies at 12.5 and 8.75 Hz (10 Hz) and 7.5 and 4.4 Hz (5 Hz). These frequencies were chosen to be representative of high frequency P-wave propagation and lower frequency SV-wave propagation on the vertical component as discussed in Section 3. In addition, some time histories were band-pass filtered at a higher frequency where the V/H ratio was larger than 1, this occurred when the V/H ratio was less than 1 at both 10 and 5 Hz.

The largest positive peak of the cross-correlation function gives the lag-time between the depths at which the vertical time histories are most similar. The lag-time in this case can be interpreted as the propagation delay time between the two depths. Then, the vertical distance between the two channels divided by the lag-time gives an estimate of the average propagation velocity between the depths.

This analysis is limited in accuracy by the time sample interval (dt) of the recorded time histories (see Table 2). For example, the Treasure Island array has a time sample interval of 0.01 sec. If the cross-correlation lag-time between the surface and 122m is 0.05 seconds then an estimate of the velocity is 2440 m/sec. However, a lag-time of 0.05 seconds is only constrained to the range 0.045 to 0.055 due to the dt of 0.01 second. Hence, the estimated velocity is in the range from 2220 to 2710 m/sec. This effect becomes pronounced as the lag-time decreases to 0.0 second. In this case, the range is from 24400 m/sec to infinite velocity.

A subset of the array data were analyzed using cross-correlation analysis. Array events were chosen provided they had similar characteristics to the design parameters for the San Francisco - Oakland Bay Bridge, that is, they recorded large magnitude crustal earthquakes ($M \geq 6.9$) with peak accelerations greater than 0.1 g (Kainan, LSST-Lotung, Port Island, Takasago, Techcent) or had similar sub-surface profiles (Treasure Island). These cross-correlations generally give velocity estimates that are near the average P-wave profile velocity or greater at all frequencies analyzed (Table 2).

Figures 14 through 16 show the cross-correlation function for channel 2 (vertical time history recorded at the surface) and channel 28 (vertical time history recorded at 122 m) for the August 18, 1999 earthquake recorded at the Treasure Island array. The first second of the cross-correlation function is plotted. The frequencies chosen are 22, 10 and 5 Hz. Figure 17 is the V/H ratio at the surface for this earthquake and shows that the V/H ratio is lower than one at 5 and 10 Hz but larger than one at 22 Hz.

The estimated propagation velocities from the cross-correlation are 2033, 2400 and 2440 m/sec at 22, 10 and 5 Hz, respectively (Table 2). The range of velocity for 10 and 5 Hz, based on a time sample size of 0.01 second, is from 2218 to 2711 m/sec. All of the cross-correlation

velocities are within 30% of the average P-wave of 1920 m/sec measured in the profile from the surface to 122m. The average S-wave velocity in the profile for the same depth range is much smaller, only 310 m/sec.

4.3 Uphole Velocity From Travel-Time Of the Initial P-wave Arrival At The Array As A Function Of Depth

A time domain measurement of the vertical propagation velocity of the high-frequency P-wave energy on the vertical component can be made by determining the time of the P-wave arrival at depth and at the surface. The vertical distance between the sensors divided by the difference in the arrival times is an estimate of the average profile P-wave velocity. As expected, when the P-wave arrivals were significantly above the noise level this measure gave a velocity close to the average P-wave velocity from the profile. Figures 18 and 19 show the P-wave first arrival on the vertical component and the S-wave first arrival on a horizontal component, respectively. The P-wave velocity from the first arrival is 2560 m/sec which is close to the cross-correlation velocities (Table 2). The S-wave velocity from the first arrival is 300 m/sec. These velocities compare favorably with the average velocities estimated from the profile of 1920 and 310 m/sec.

4.4 Short-Period Time Domain

To perform a short-period time domain analysis similar to Section 3.1 an array is selected for analyses provided that it has a sensor located in competent rock and recorded earthquakes at both close-in fault ($\leq$ 10 to 15 km) and greater distances. The Garner Valley and Treasure Island arrays are the only arrays that have rock recordings, in granite (220 m) at Garner Valley, and in shale at a depth of 122 m at Treasure Island. However, the closest earthquakes to these arrays occurred at hypocentral distances (see Table 1) of greater than 14 km, and these distances are unfortunately probably in the transition region from close-in to more distant rock site characteristics and beyond.

The accelerograms from the three closest and best-recorded (adequate signal-to-noise for this analysis) earthquakes at Treasure Island array are analyzed. The Treasure Island array data were selected because the array has the most recordings with depth, and is representative of soil sites along the San Francisco - Oakland Bay Bridge. The following acceleration time history plots illustrate general trends in short period vertical and horizontal motions recorded as discussed in Section 3.1.

To illustrate these effects on acceleration time histories for vertical and horizontal components recorded at the Treasure Island array, a series of plots with the vertical component at 0, 7, 16, 31, 44, and 122 (or 104) m depth are shown (Figures 20, 22 and 24). The corresponding horizontal time histories provide the S waveform, arrival time and phasing information (Figures 21, 23 and 25). In order to present some of the low amplitude accelerograms recorded at depth along with higher amplitude surface recordings the amplitude scale may differ from component to component on these figures.

Figures 20 and 21 are acceleration time histories from the 06/26/94 ML 4.0 earthquake located at 14.2 km hypocentral distance from the Treasure Island array. At this time, the deepest

sensor was located in weathered rock at 104 m depth. On the vertical component (Figure 20) the P-wave arrival near 2.5 seconds is of similar amplitude as the SV-wave arrival near 4.5 seconds at both the weathered rock and soil sites. As expected, upon detailed examination, at 104 m (rock) the SV-wave amplitude is slightly larger than the P-wave amplitude, while at the surface (soil), the opposite is observed. In addition, the surface vertical accelerogram is richer in higher frequencies near 25 Hz than the other soil accelerograms.

Figures 22 and 23 are accelerograms from the 12/04/98 ML 4.1 earthquake located at 14.7 km hypocentral distance. The deepest sensor is located in rock at 122 m depth. Similarly, an impulsive P-wave arrival near 4.7 seconds on the vertical component (Figure 22) is generally of similar amplitude as the SV-wave arrival near 6.9 seconds at both the rock and soil sites. A possible explanation is that these records appear to be in the transition zone from close-in to more distant site characteristics.

The accelerograms from the 08/18/99 ML 5.0 earthquake located at 29.8 km hypocentral distance are shown in Figures 24 and 25. The rock sensor is at 122 m depth. An Interesting and apparent contradiction is that on the vertical component (Figure 24) the SV-wave tends to dominate at both rock and soil sites. Radiation pattern effects may explain this discrepancy.

In summary, the trends observed in Section 3.1 for surface recordings from large earthquakes are not as clearly observed from these smaller and more distant array recordings at Treasure Island. However, the results are encouraging especially for the closest recording at 14.2 km (Figures 20 and 21).

4.5 Amplitude Trends with Depth

In general, both the horizontal and vertical spectral and time domain amplitudes decrease as depth increases. The increase in amplitude near the surface is caused, in general, by a doubling of amplitude at the free surface, and the increase in wave amplitude with decreasing media velocity. Figures 20 to 25 illustrate this wave propagation property in the time domain at Treasure Island. Recall that the amplitude scale changes between the time histories which has the effect of increasing the plotted amplitude of the deeper recordings. In the spectral domain, Figure 26 shows the average horizontal spectra normalized by the average surface horizontal spectra as a function of depth. Figure 27 shows the corresponding plot for vertical spectra. As expected, on both of these plots the horizontal and vertical spectra generally decrease with increasing depth.

5.0 RECOMMENDATIONS FOR DESIGN

From the analysis of vertical array ground motion data, the following two recommendations are made:

1) In developing vertical motions from horizontal motions, the use of the surface V/H ratio for V/H ratios at various depths is conservative at high frequencies (> 10 Hz) but is not conservative at low frequencies, generally less than about 10 Hz, as the at-depth V/H spectral ratio is larger than at the surface at low frequency. As a result, applying a surface V/H ratio to at-depth horizontal spectra to develop at-depth vertical loads is not recommended. Unless a reliable at-

depth V/H ratio is available, at-depth vertical motions should be developed by applying the surface V/H ratio to surface horizontal spectra and then adjusting the resulting surface vertical spectra for depth effects (if any). Our analyses suggest that this approach is likely conservative but is only appropriate if the at-depth horizontal motions are smaller than those at the surface.

2) The velocity at which the high-frequency (> 5 to 10 Hz) vertical ground motion propagates up a vertical array is near the average P-wave velocity of the subsurface materials. Both cross-correlation and first arrival analyses are in general agreement.

6.0 REFERENCES

Bozorgnia, Y., M. Niazi, and K. W. Campbell (1995). "Characteristics of free-field vertical ground motion during the Northridge earthquake." *Earthquake Spectra,* 11(4), 515-525.

Darragh, R., M. Huang, and A. Shakal (1993). "Processed strong-motion records from the CSMIP\NSF Treasure Island Geotechnical Array for the Gilroy Earthquake of 16 January 1993", Division of Mines and Geology, Office of Strong Motion Studies Report, OSMS 93-09, 37 pp.

Electric Power Research Institute (1993). "Guidelines for determining design basis ground motions." Palo Alto, Calif: Electric Power Research Institute, vol. 1-5, EPRI TR-102293.

Niazi, M. and Y. Bozorgnia (1991). "Behavior of near-source peak horizontal and vertical ground motions over SMART-1, array, Taiwan." *Bull. Seism. Soc. Am.,* 81(3), 715-732.

Steidl, J. H., A. G. Tumarkin, and R. J. Archuleta (1996). "What is a Reference Site?" *Bull. Seism. Soc. Am.*, 86(6), 1733-1748.

Table 1

VERTICAL ARRAY STRONG-MOTION CATALOG (08/10/99) - ANALYZED DATA

Vertical Array		Date & Time YEAR	MODY	HRMN	Magnitude	Epicentral Dist.(km)	Source Depth (km)	Sensor Depths
CHIBA, Japan	EQ8307	1983	0227		6.0 (Mjma)	35	72	1, 5, 10, 20, 40m
	EQ8420	1984	1217		4.9 (Mjma)	5	78	
	EQ8510	1985	0608		4.8 (Mjma)	16	64	
	EQ8519	1985	1004		6.1 (Mjma)	28	78	
	EQ8525	1985	1106		5.0 (Mjma)	32	63	
	EQ8722	1987	1217		6.7 (Mjma)	45	58	
	EQ8806	1988	0116		5.2 (Mjma)	38	48	
	EQ8816	1988	0318		6.0 (Mjma)	42	96	
	EQ8901	1989	0219		5.6 (Mjma)	48	55	
Garner Valley	E01	1989	1202	2316	4.2 (ML)	6.2	14.5	0, 6, 15, 22, 55, 220m
	E02	1989	1222	0303	3.4 (ML)	5.4	14.1	
	E07	1992	0424	0225	4.6 (ML)	45.9	11.9	
	E08	1992	0424	0450	6.1 (ML)	46.2	12.4	
	E09	1992	0427	0955	3.6 (ML)	42.0	6.6	
	E10	1992	0505	0116	4.1 (ML)	42.9	6.0	
	E11	1992	0505	1619	4.9 (ML)	45.6	12.5	

Table 1 (cont.)

VERTICAL ARRAY STRONG-MOTION CATALOG (08/10/99) - ANALYZED DATA

Vertical Array	Date & Time YEAR	MODY	HRMN	Magnitude	Epicentral Dist.(km)	Source Depth (km)	Sensor Depths
E12	1992	0507	0238	4.7 (ML)	45.0	7.3	
E13	1992	0519	1544	4.9 (ML)	44.1	7.1	
E14	1992	0630	1408	5.6 (ML)	54.5	10.4	
E15	1992	0630	1413	5.4 (ML)	54.8	9.9	
E17	1992	0701	2123	4.8 (ML)	51.6	12.5	
E18	1992	0706	0418	3.1 (ML)	2.2	17.8	
E21	1993	0425	1630	2.3 (ML)	4.9	12.3	
E25	1994	0422	0233	2.5 (ML)	8.5	13.3	
E28	1994	1109	0229	3.7 (ML)	11.6	17.2	
Kainan, Japan	1995	0116		6.9 (M)	44.7	10.0	0, 25, 100m
La Cienega	1995	0626		5.0 (ML)	47.6	13.3	0, 18, 101, 252m
	1997	0318		5.1 (ML)	176.7	1.8	
	1997	0404		3.3 (ML)	6.7	4.2	
	1997	0405		2.5 (ML)	6.4	4.1	
	1997	0426		5.1 (ML)	45.8	16.5	

Table 1 (cont.)

VERTICAL ARRAY STRONG-MOTION CATALOG (08/10/99) - ANALYZED DATA

Vertical Array	Date & Time YEAR	MODY	HRMN	Magnitude	Epicentral Dist.(km)	Source Depth (km)	Sensor Depths
	1997	0427		4.9 (ML)	45.7	15.2	
	1998	0112		3.4 (ML)	19.1	11.3	
	1998	0415		3.2 (ML)	13.0	9.2	
	1999	0617		3.0 (ML)	14.7	4.6	
LSST-Lotung, Taiwan	1986	0329	0717	4.7 (ML)	13		0, 6, 11, 17, 47m
	1986	0520	0526	6.4 (Ms)	67	16	
	1986	0717	0003	5.0 (ML)	5	2	
	1986	0730	1131	5.6 (Ms)	6	2	
	1986	0730	1138	4.9 (ML)	5	2	
	1986	0805	0056	4.9 (ML)	5		
	1986	1114	2120	7.8 (Ms)	79	7	
Port Island, Japan	1995	0116		6.9 (M)	2.5	10.0	0, 16, 32, 83m
	1995	0118	0525	3.0 (M)	1.1	9.6	
	1995	0126	0101	3.3 (M)	2.2	11.0	

Table 1 (cont.)

VERTICAL ARRAY STRONG-MOTION CATALOG (08/10/99) - ANALYZED DATA

Vertical Array	Date & Time YEAR	MODY	HRMN	Magnitude	Epicentral Dist.(km)	Source Depth (km)	Sensor Depths
	1995	0202	1257	2.4 (M)	4.0	5.9	
	1995	0202	1604	3.4 (M)	16.2	12.8	
	1995	0202	1619	3.4 (M)	3.6	17.2	
	1995	0203	2036	3.0 (M)	7.1	5.2	
	1995	0218	2137	3.8 (M)	39.3	20.4	
Takasago, Japan	1995	0116		6.9 (M)	25.6	10.0	0, 25, 100m
Techcent, Japan	1995	0116		6.9 (M)	7.4	10.0	0, 25, 100m
Treasure Island	1993	0116		5.3 (ML)	120.4	7.9	0, 7, 16, 31 44, 104, 122m
	1994	0626		4.2 (ML)	12.6	6.6	
	1998	0812		5.4 (ML)	143.8	9.2	
	1998	1204		4.1 (ML)	13.0	6.9	
	1999	0818		5.0 (ML)	29.0	6.9	
Wildlife Liquefaction	1987	1124		6.2 (M)	24	10.6	0, 7.5m
	1987	1124		6.6 (M)	32	1.9	

Table 2

CROSS-CORRELATION VELOCITIES COMPARED TO AVERAGE PROFILE VELOCITIES FROM VERTICAL STRONG-MOTION ARRAY DATA

Vertical Array Location	Frequency (Hz)	V/H ratio of surface sensors	Cross-Correlation Velocity (Range) (m/sec)*	Average Measured Profile Velocity#		Comparison to Profile Velocity##
				P-wave (m/sec)	S-wave (m/sec)	
Kainan	15	>1	1667 (1820-1540)	1751	291	P-wave
	10	<1	1667 (1820-1540)			P-wave
	5	<1	2000 (2220-1820)			~ P-wave
Tagasago	10	>1	833 (870- 800)	1322	339	>>S-wave, < P-wave
	5	<1 (0.9)	1000 (1050- 950)			>>S-wave, < P-wave
Techcent	10	<1	2000 (2220-1820)	1588	279	> P-wave
	5	<1	1428 (1540-1333)			~ P-wave
Port Island	26	>1	1186 (1280-1110)	1222	246	P-wave
	10	<1	1037 (1110-976)			~ P-wave
	5	<1	922 (980-870)			< P-wave
LSST-Lotung	10	>1	566 (620-520)	1201	226	>>S-wave, <<P-wave
(Event 16)	5	>1	1700 (2270-1360)			> P-wave

Table 2 (cont.)

CROSS-CORRELATION VELOCITIES COMPARED TO AVERAGE PROFILE VELOCITIES FROM VERTICAL STRONG-MOTION ARRAY DATA

Vertical Array Location	Frequency (Hz)	V/H ratio of surface sensors	Cross-Correlation Velocity (Range) (m/sec)*	Average Measured Profile Velocity#		Comparison to Profile Velocity##
				P-wave (m/sec)	S-wave (m/sec)	
Treasure Island	24	>1	1040 (1090-990)	1755	270	>>S-wave, < P-wave
06/26/94	10	<1	2080 (2311-1890)			~P-wave
	5	<1	520 (530-510)			>S-wave, <<P-wave
Treasure Island	22	=1	2033 (2220-1880)	1920	310	P-wave
12/04/98	10	<1	2440 (2710-2220)			~P-wave
	5	<1	2440 (2710-2220)			~P-wave
Treasure Island	22	>1	2033 (2220-1880)	1920	310	P-wave
08/18/99	10	<1	2440 (2710-2220)			~P-wave
	5	<1	2440 (2710-2220)			~P-wave

*The cross-correlation velcocity is from the deepest sensor to the surface:
Kainan, Tagasago, and Techcent are measured from 100 m to the surface. Port Island is measured from 83 m to the surface. LSST-Lotung is measured from 17 m to the surface. Treasure Island is measured from 104 m (1994 earthquake) or 122m (1998 and 1999 earthquakes) to the surface.
The range of cross-correlation velocities is calculated from velocity (min, max) = depth / (lag time +- 0.5 dt).
The time sample interval (dt) from the processed time histories is: 0.01 sec for Kainan, Tagasago, Techcent, Port Island, and Treasure Island, arrays and 0.005 sec for LSST-Lotung.

#The measured P-wave and S-wave velcoity profiles are shown in Appendix A for the arrays.

The following symbols are used for the comparison, for cases when the range of the cross-correlation velocity:
1) includes the average measured profile velocity then the wave type is listed.
2) is within +- 20 % of the average measured profile velocity then a (~ symbol) is used in front of the appropriate wave type.
3) is greater (or lesser) than +- 20% but within a factor of 2 of the average measured profile velocity then a (> or < symbol) is used in front of the appropriate wave type.
4) is greater (or lesser) than a factor of 2 of the average measured profile velocity then a (>> or << symbol) is used in front of the appropriate wave type.

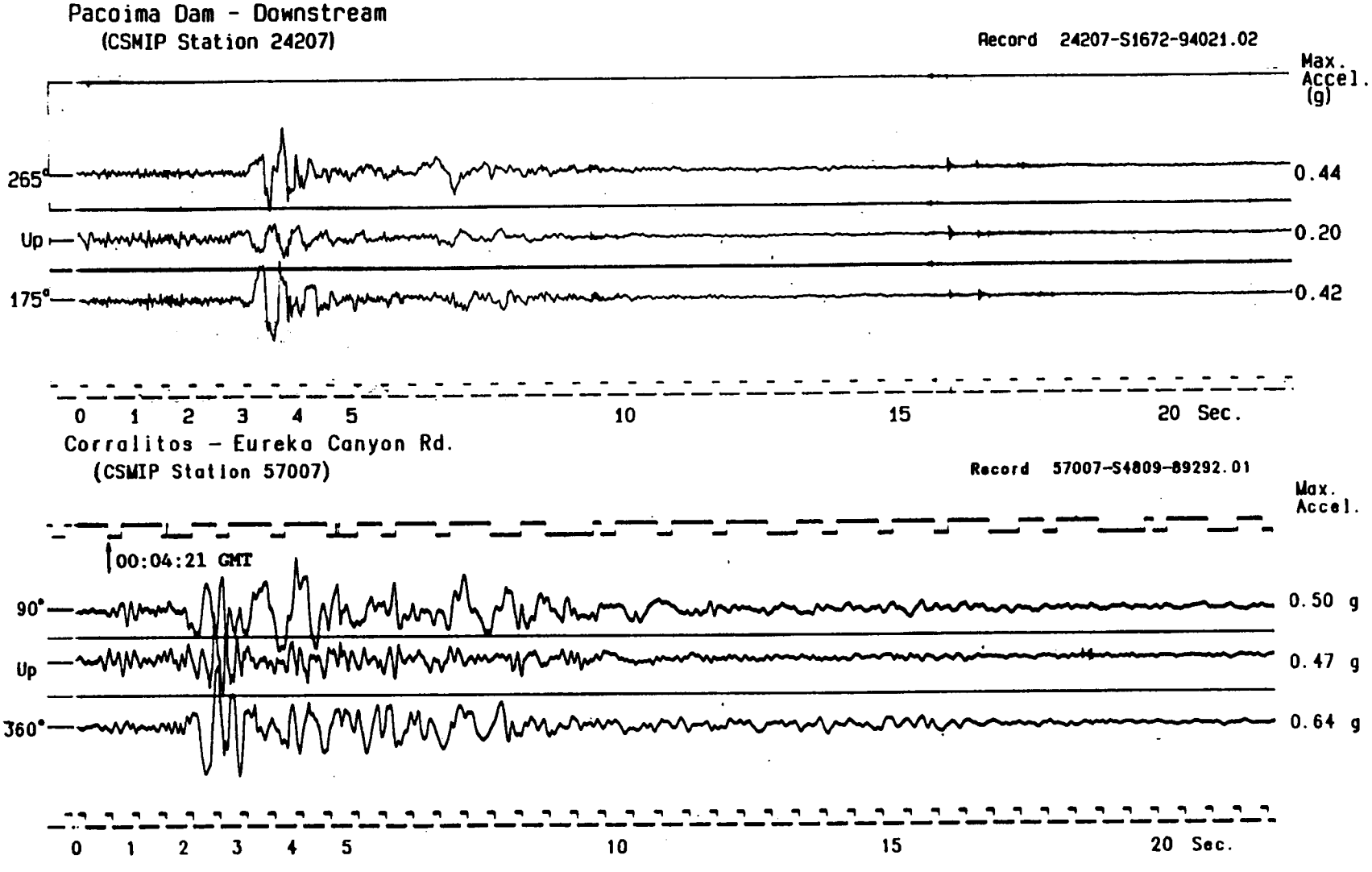

Figure 1. Horizontal and vertical component acceleration time histories recorded at rock sites Pacoima Downstream for the 1994 **M** 6.7 Northridge earthquake (top) and Corralitos for the 1989 **M** 6.9 Loma Prieta earthquake (bottom). (Source: CDMG initial data reports).

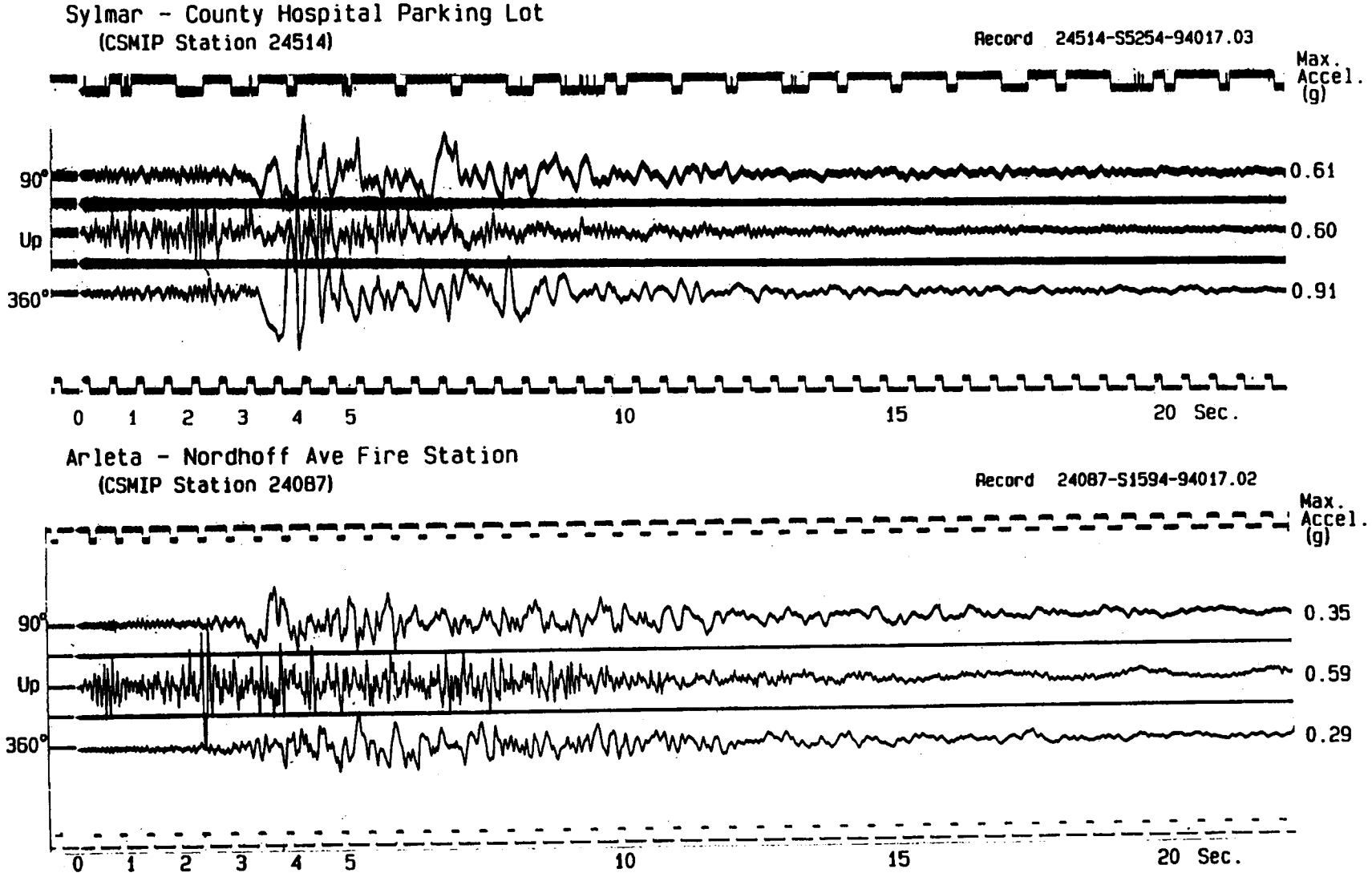

Figure 2. Horizontal and vertical component acceleration time histories recorded at soil sites Sylmar (top) and Arleta (bottom) for the 1994 **M** 6.7 Northridge earthquake. (Source: CDMG initial data reports).

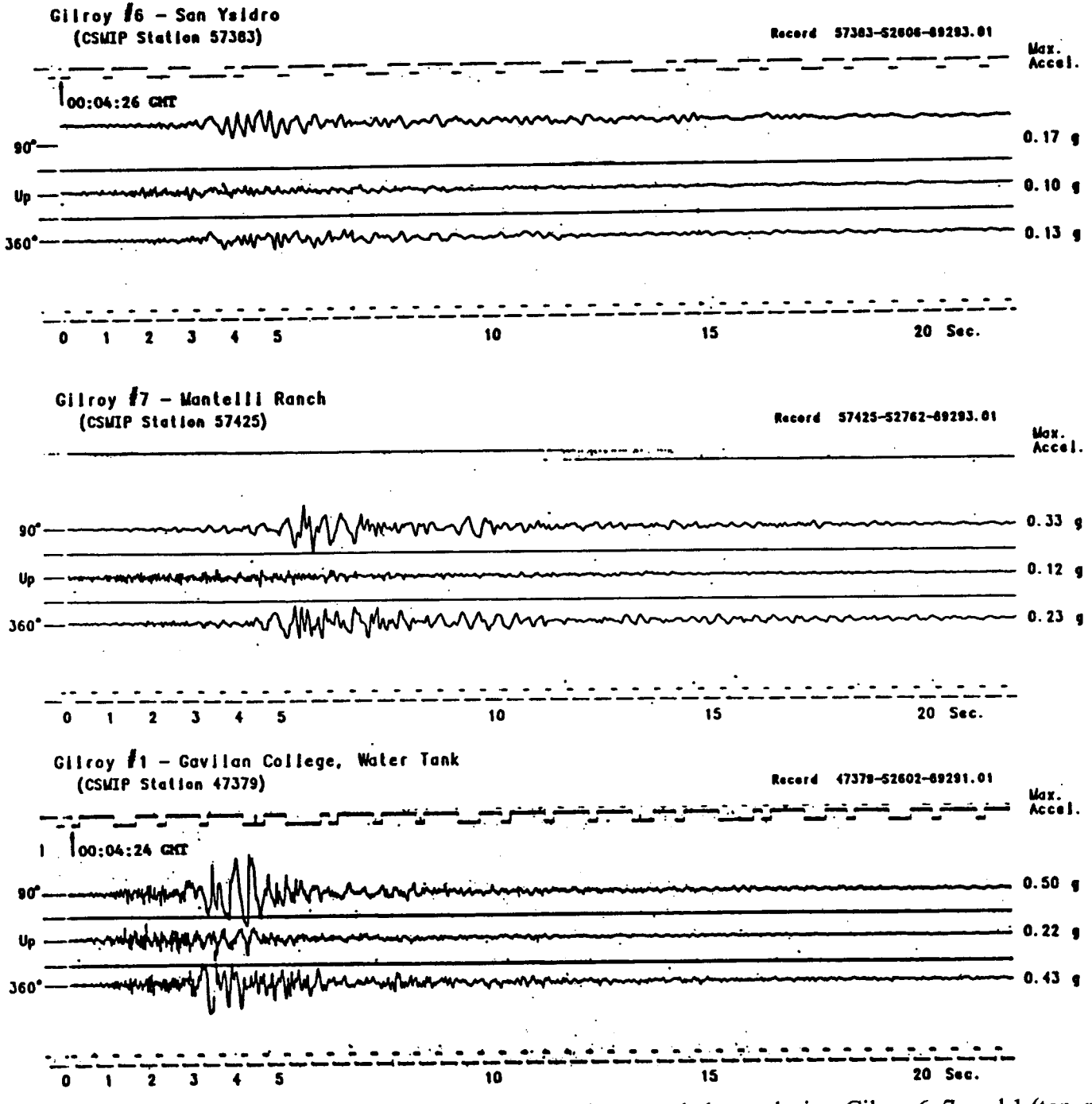

Figure 3. Horizontal and vertical component acceleration time histories recorded at rock sites Gilroy 6, 7, and 1 (top, middle, and bottom) for the 1989 M 6.9 Loma Prieta earthquake. (Source: CDMG initial data reports).

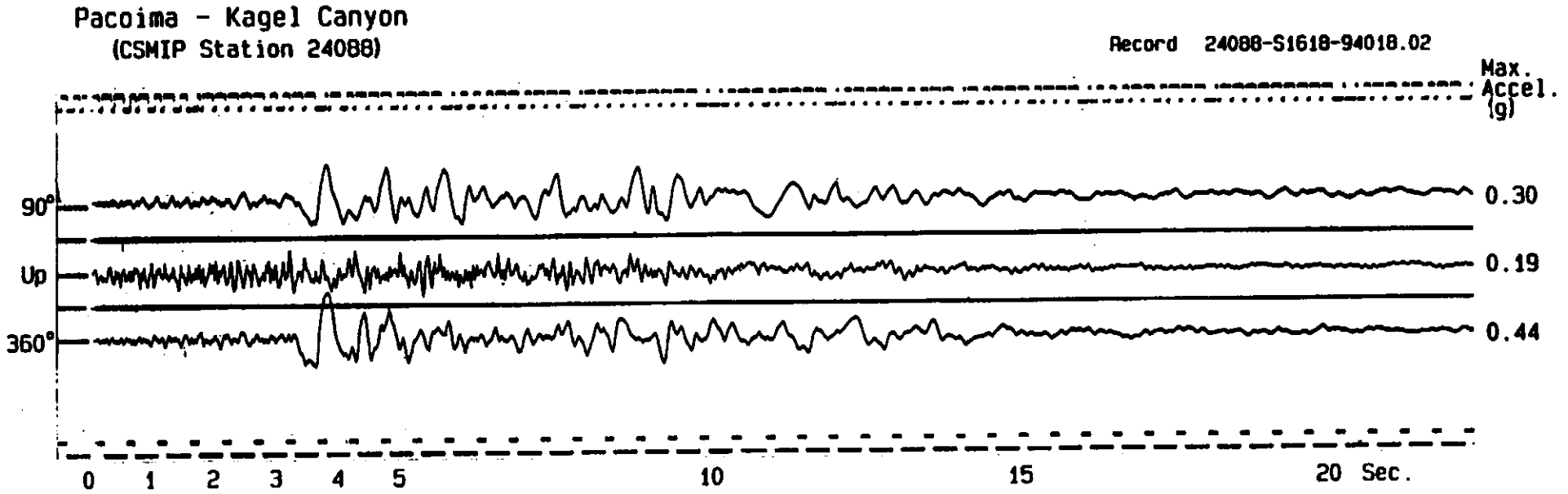

Figure 4. Horizontal and vertical component acceleration time histories recorded at "rock" site Pacoima Kagel for the 1994 **M** 6.7 Northridge earthquake. (Source: CDMG initial data reports).

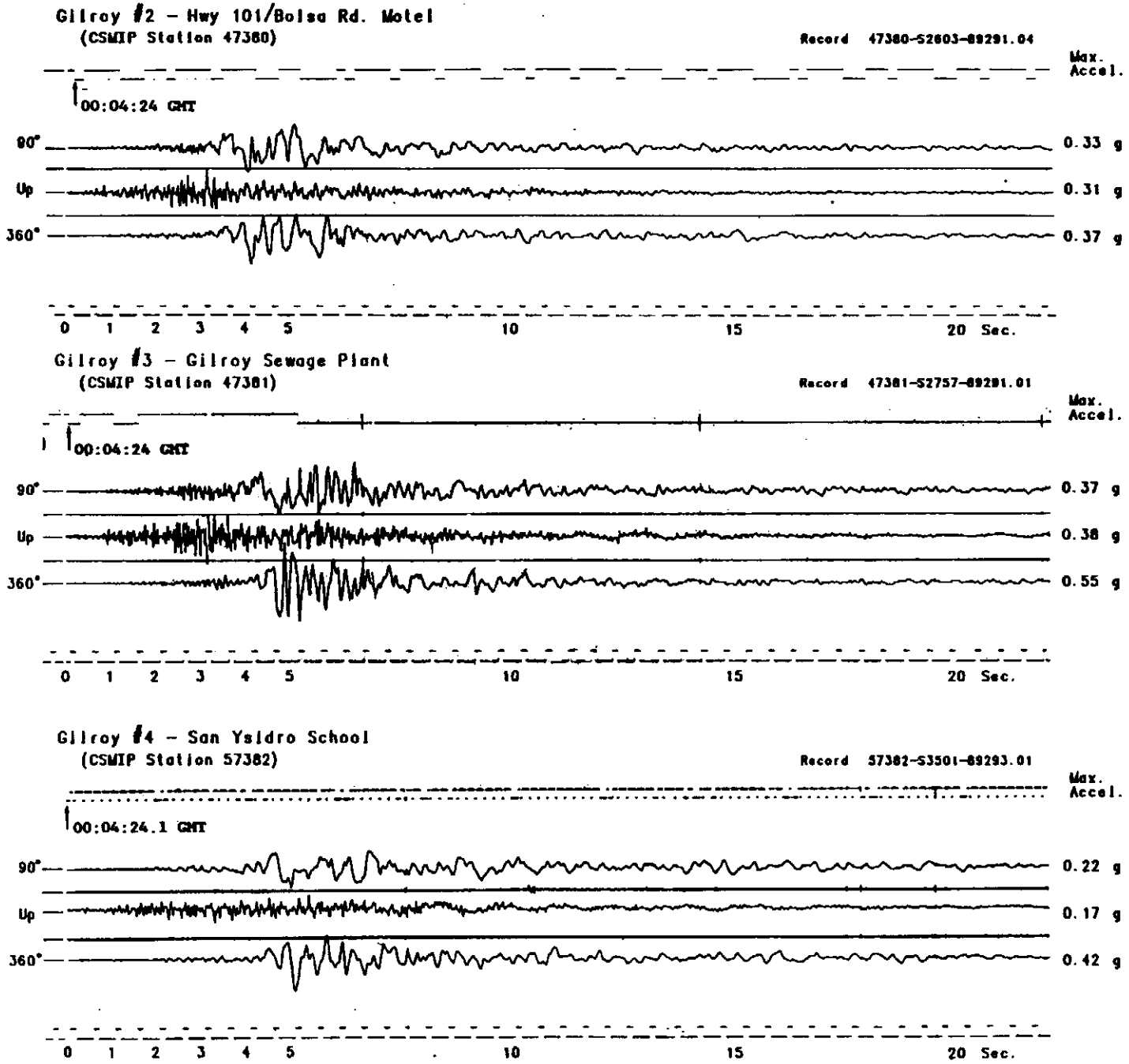

Figure 5. Horizontal and vertical component acceleration time histories recorded at soil sites Gilroy 2, 3, and 4 (top, middle, and bottom) for the 1989 M 6.9 Loma Prieta earthquake. (Source: CDMG initial data reports).

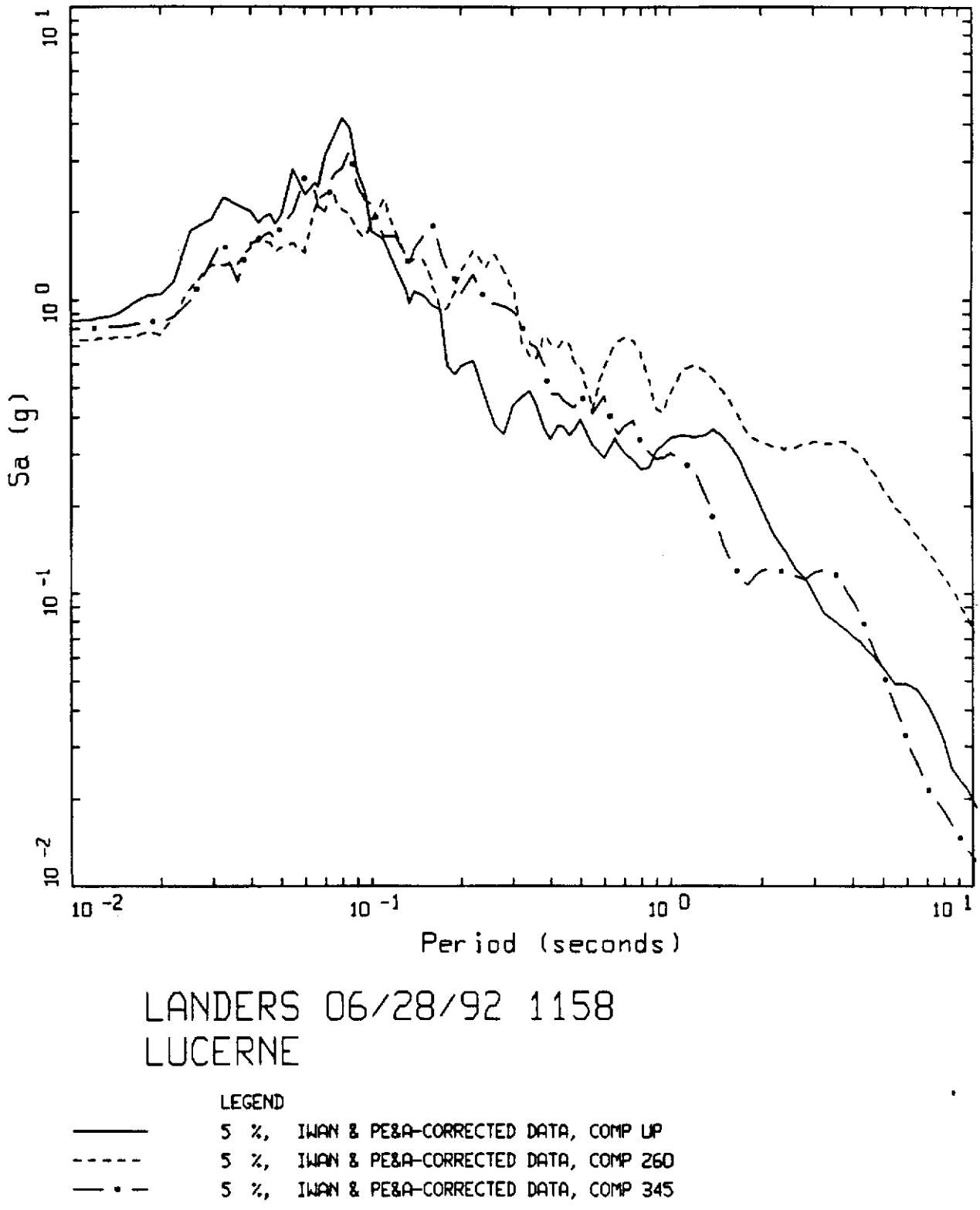

Figure 6. 5% Damped pseudo absolute response spectra at the SCE rock site Lucerne for the 1992 **M** 7.2 Landers earthquake. Fault distance is about 2 km.

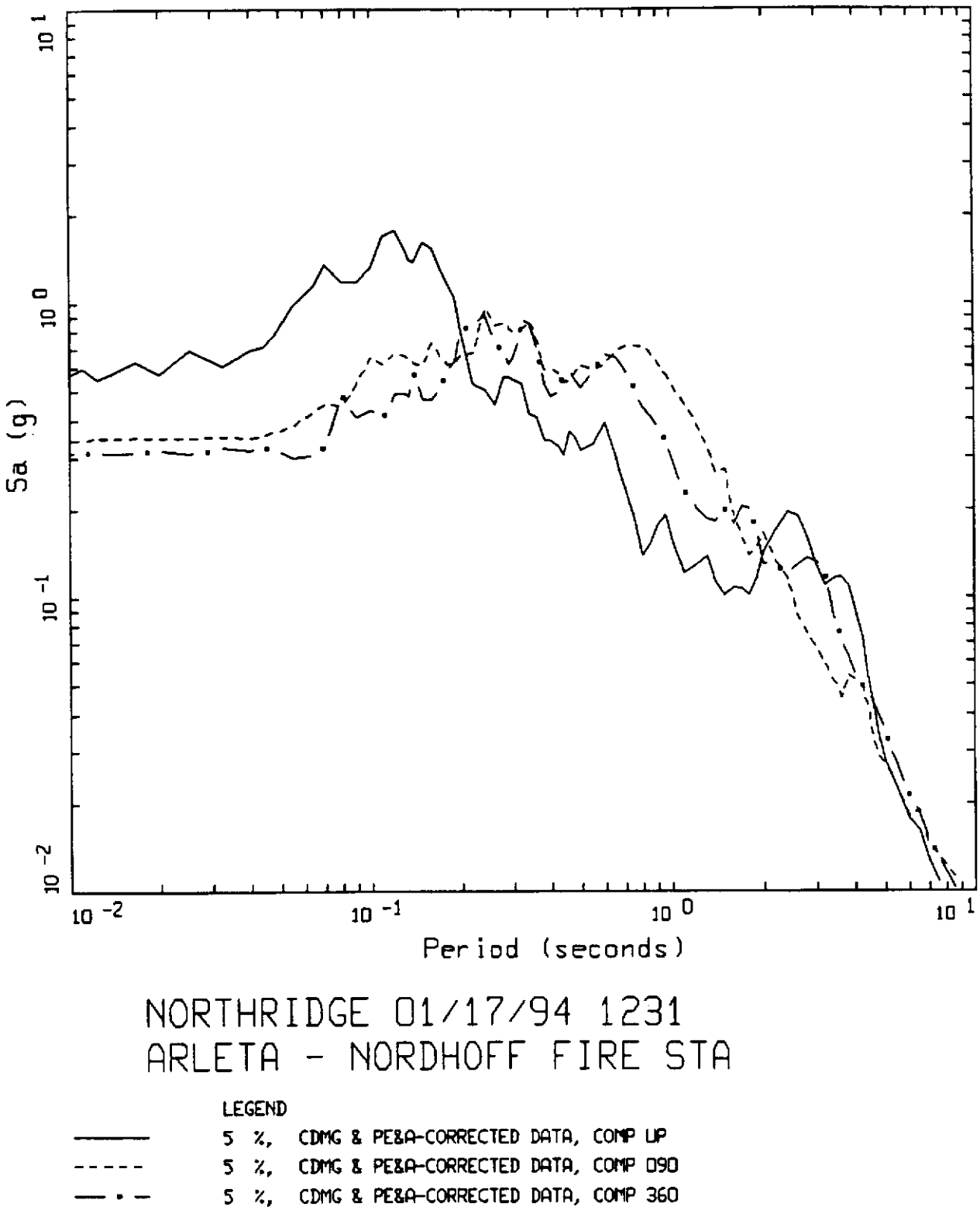

Figure 7. 5% Damped pseudo absolute response spectra at the soil site Arleta for the 1994 **M** 6.7 Northridge earthquake. Fault distance is about 9 km.

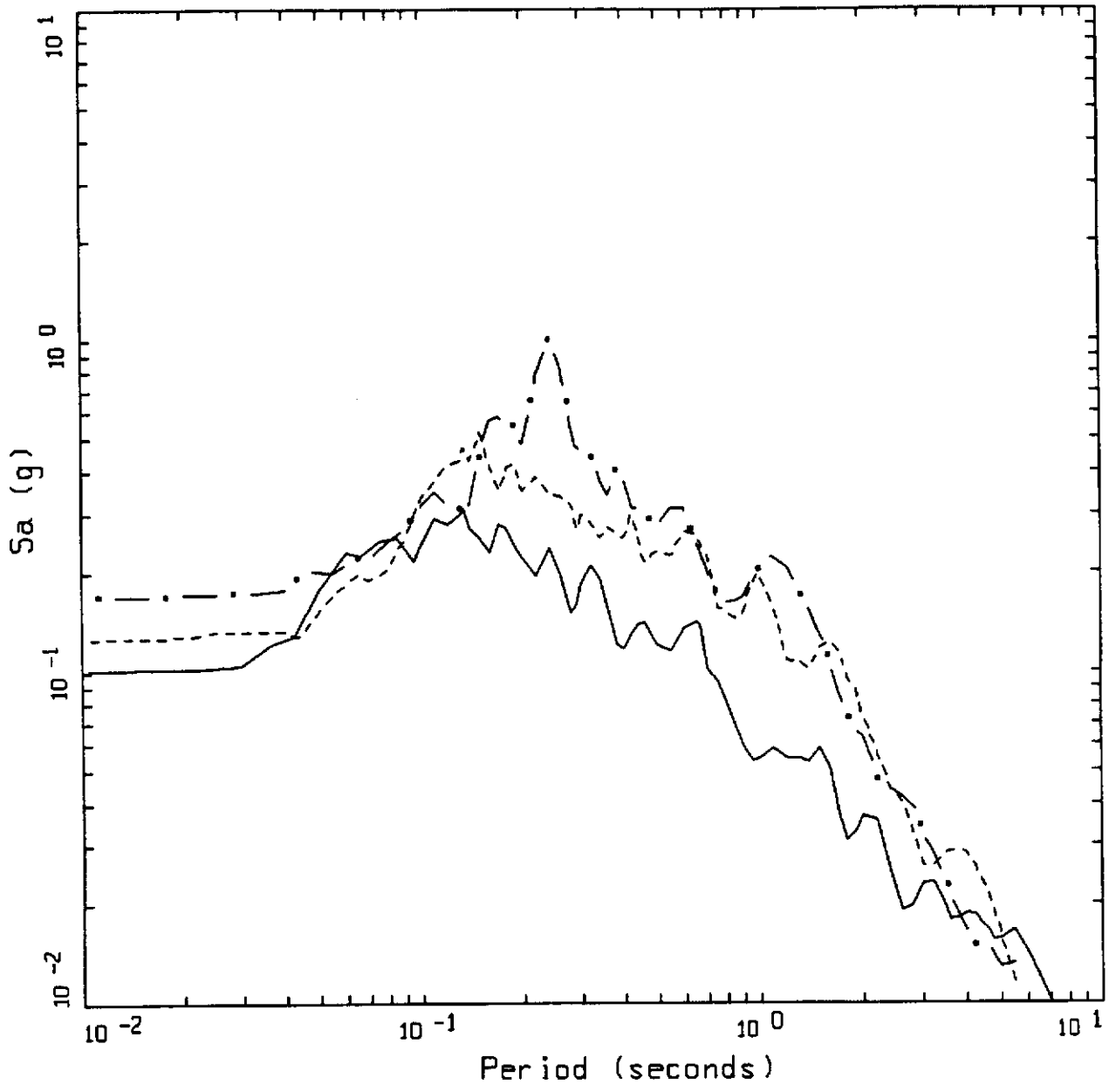

Figure 8. 5% Damped pseudo absolute response spectra at the rock site Gilroy 6 for the 1989 **M** 6.9 Loma Prieta earthquake. Fault distance is about 19 km.

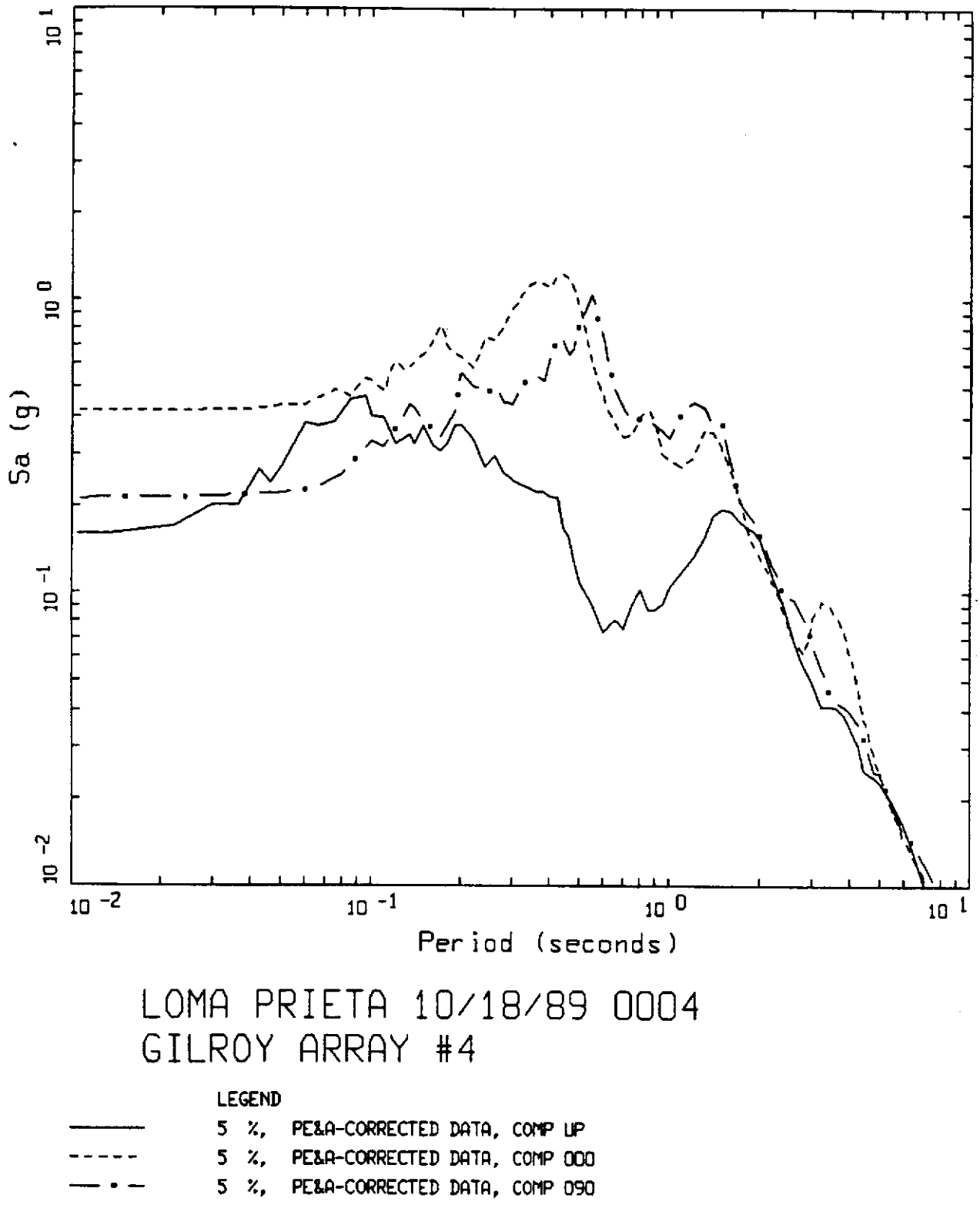

Figure 9. 5% Damped pseudo absolute response spectra at the soil site Gilroy 4 for the 1989 **M** 6.9 Loma Prieta earthquake. Fault distance is about 16 km.

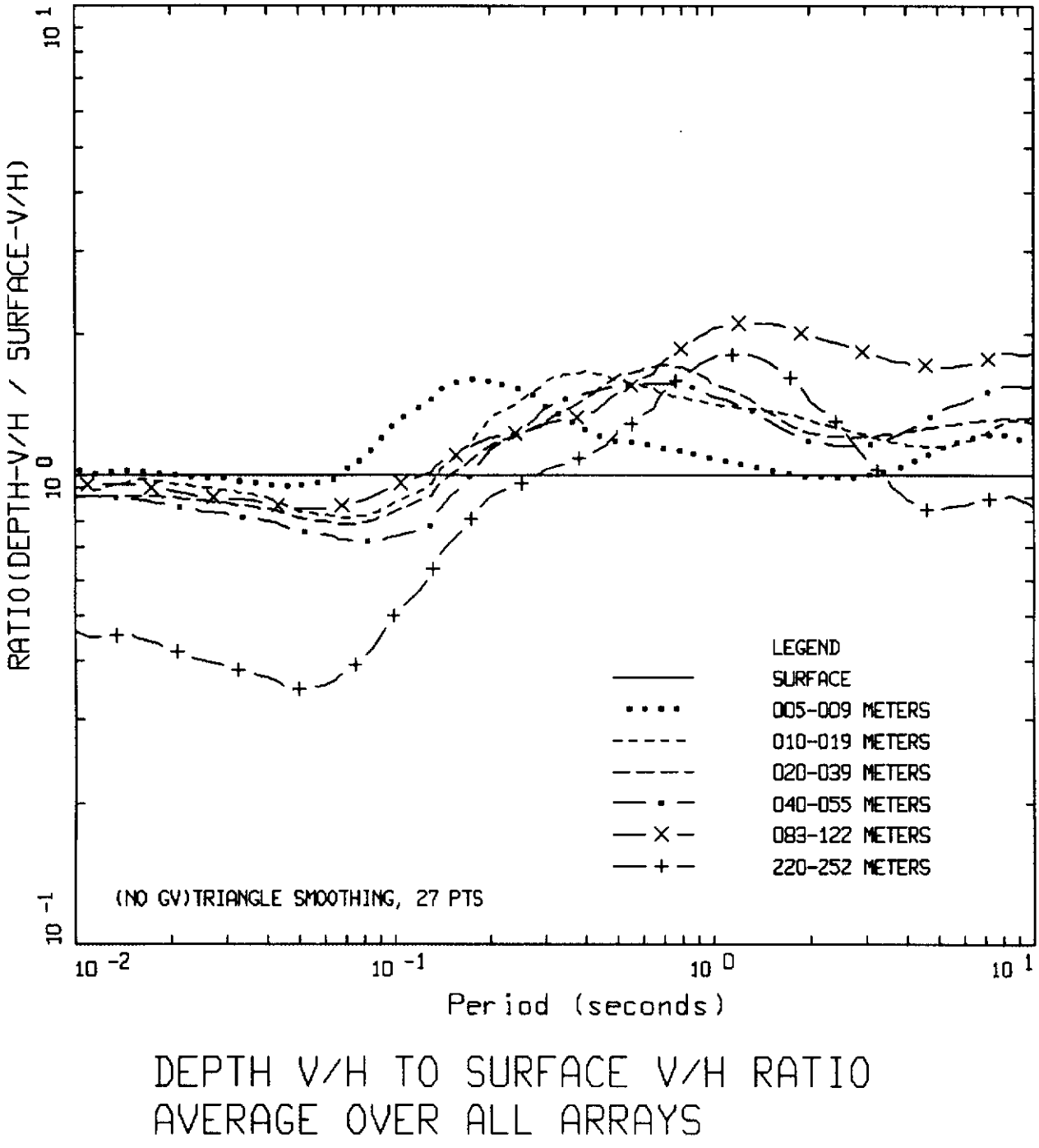

Figure 10. Normalized V/H spectral ratio (5% damping) for the surface and six depth ranges. The ratio is normalized by the surface V/H ratio and the surface ratio plots as the solid line at unity.

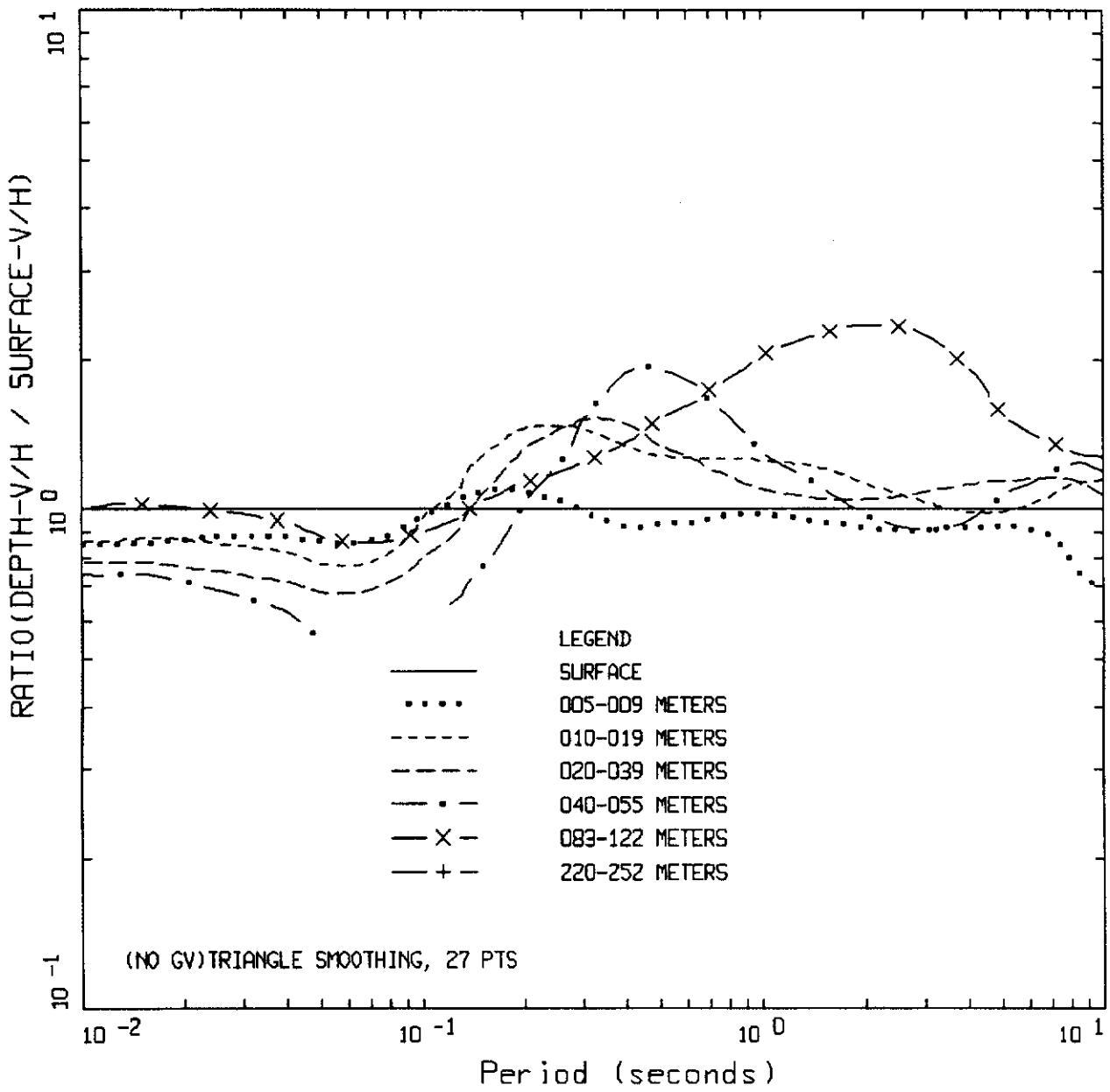

Figure 11. Normalized V/H spectral ratio (5% damping) for the surface and six depth ranges. The ratio is normalized by the surface V/H ratio and the surface ratio plots as the solid line at unity. The ratio is an average over all earthquakes with $M \geq 6$.

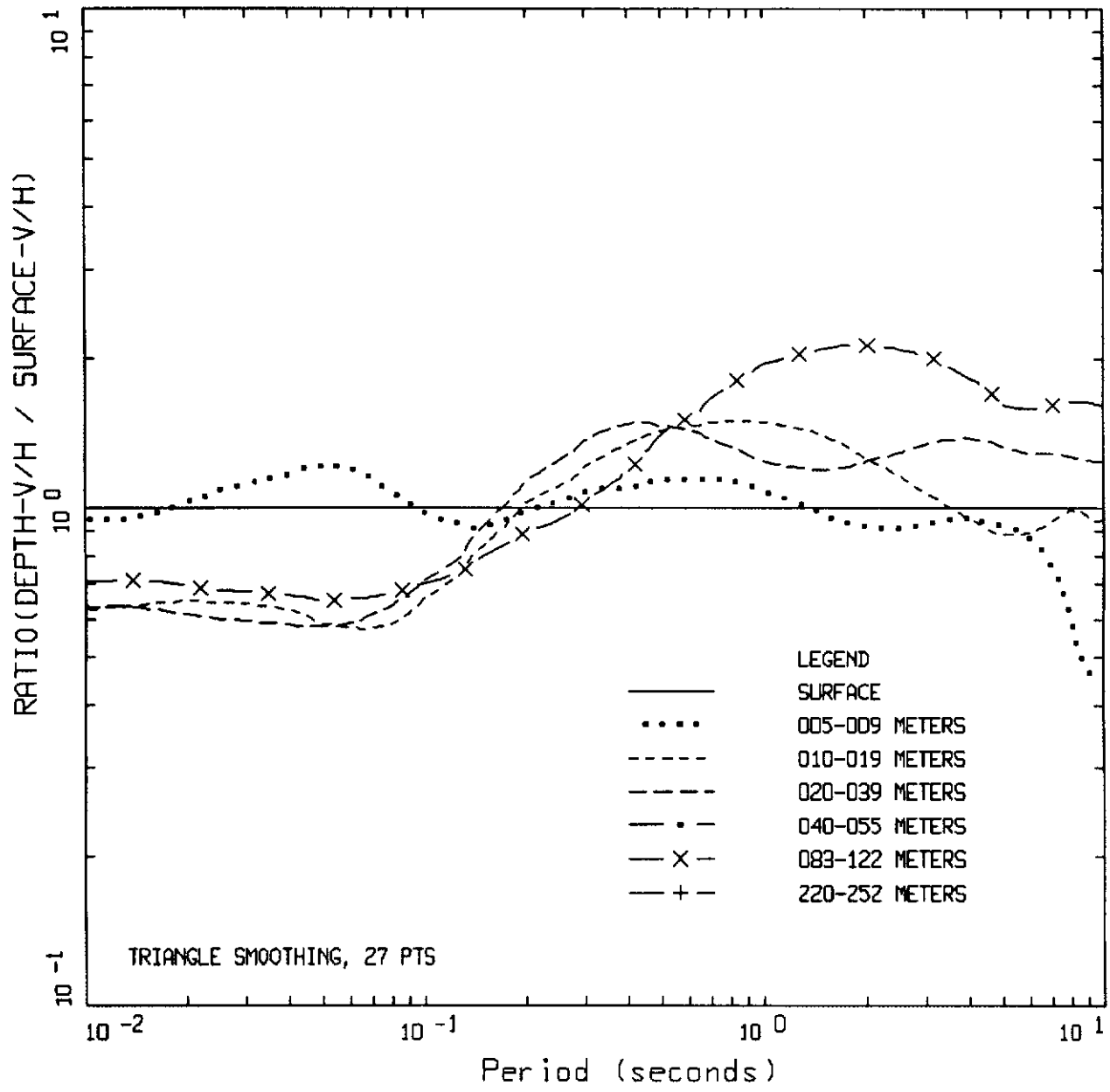

Figure 12. Normalized V/H spectral ratio (5% damping) for the surface and six depth ranges. The ratio is normalized by the surface V/H ratio and the surface ratio plots as the solid line at unity. The ratio is an average over all recordings with peak horizontal or vertical surface acceleration $\geq$ 100 cm/sec/sec, and with earthquake focal depth $\leq$ 20 km.

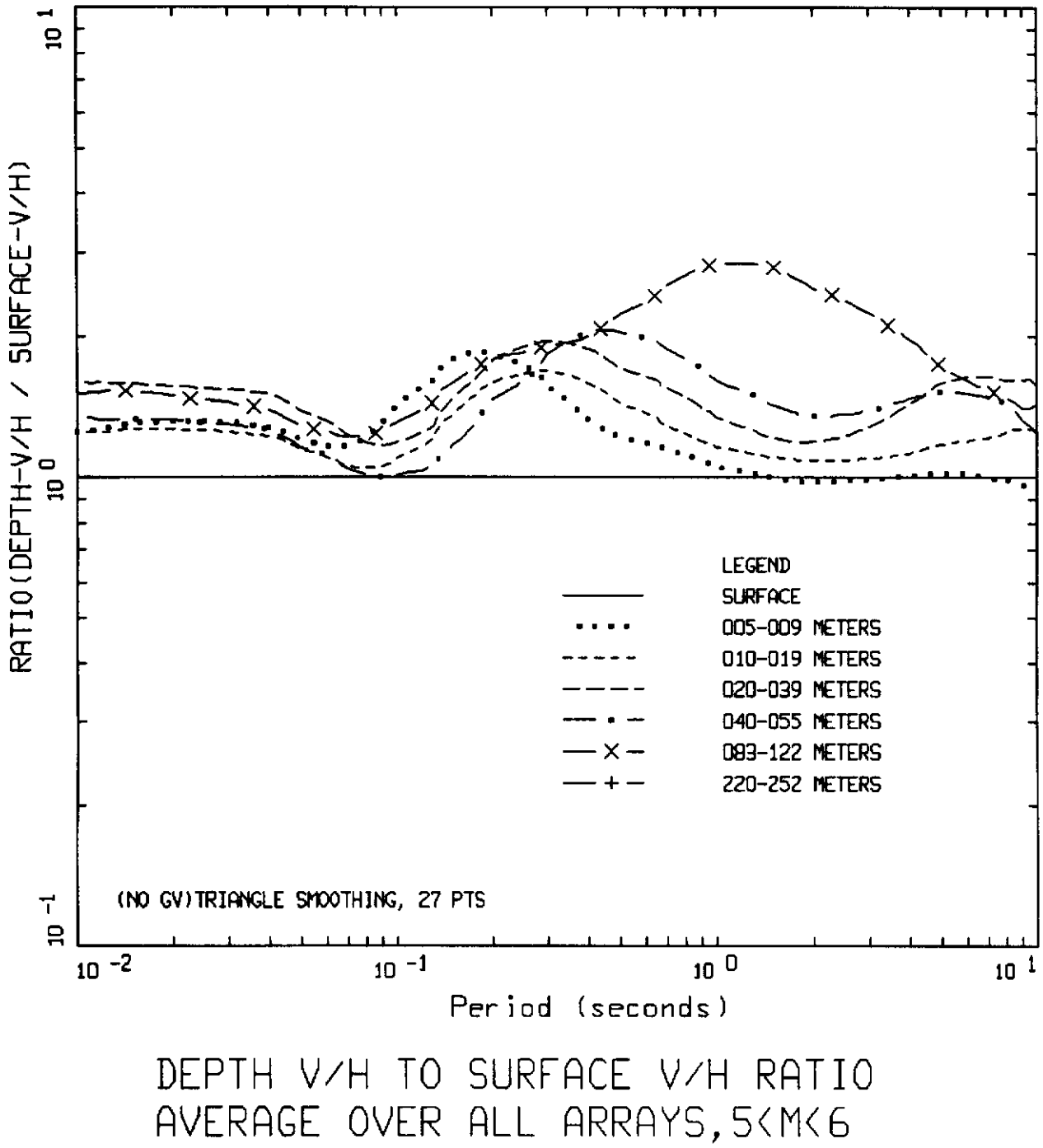

Figure 13. Normalized V/H spectral ratio (5% damping) for the surface and six depth ranges. The ratio is normalized by the surface V/H ratio and the surface ratio plots as the solid line at unity. The ratio is an average over all earthquakes with $5 \leq M \leq 6$.

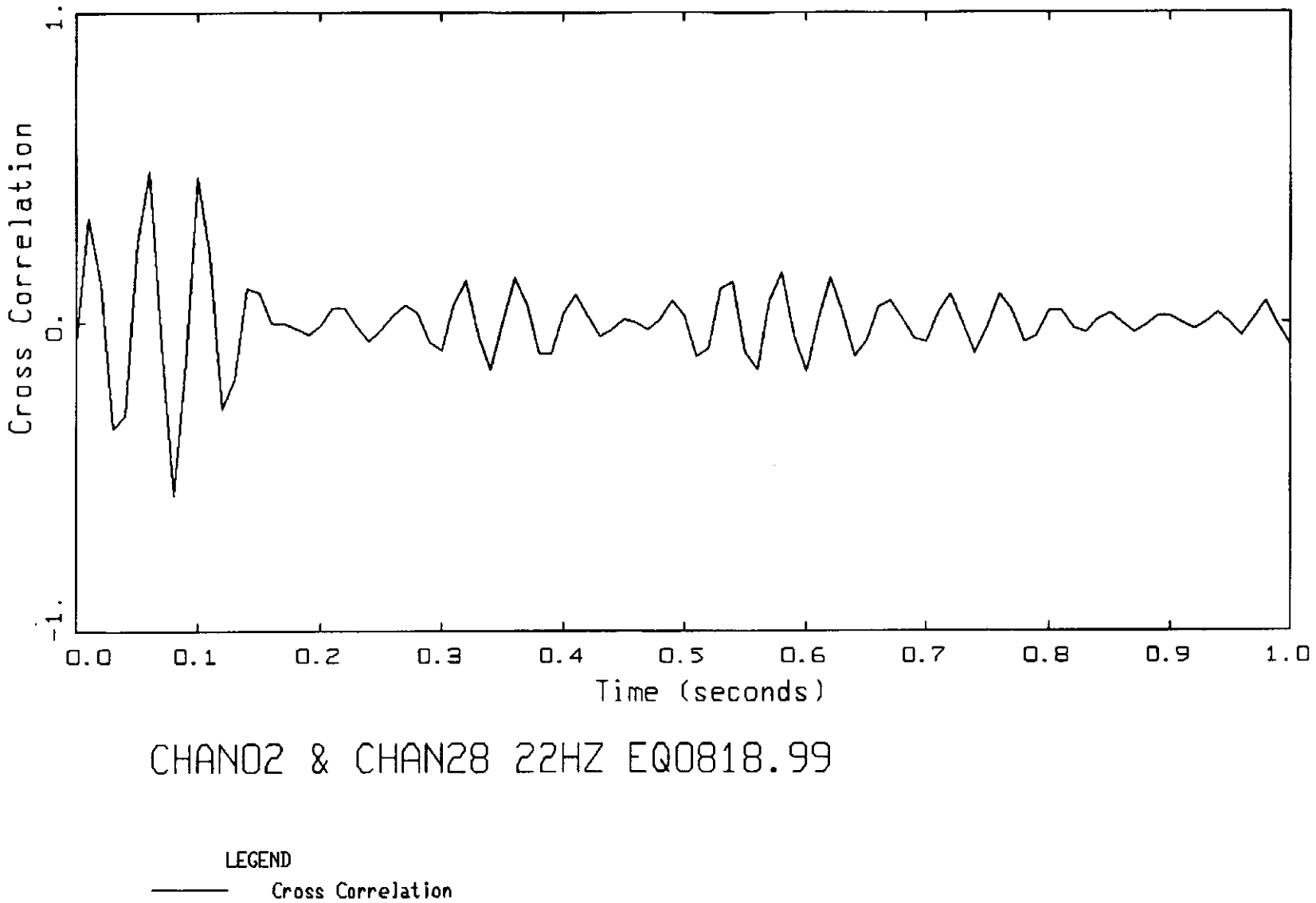

Figure 14. Cross-correlation function at 22 Hz for the vertical surface recording (Channel 2) and the rock recording at 122m (Channel 28) at Treasure Island. The magnitude 5 earthquake occurred on 8/18/99 at an epicentral distance of 29 km.

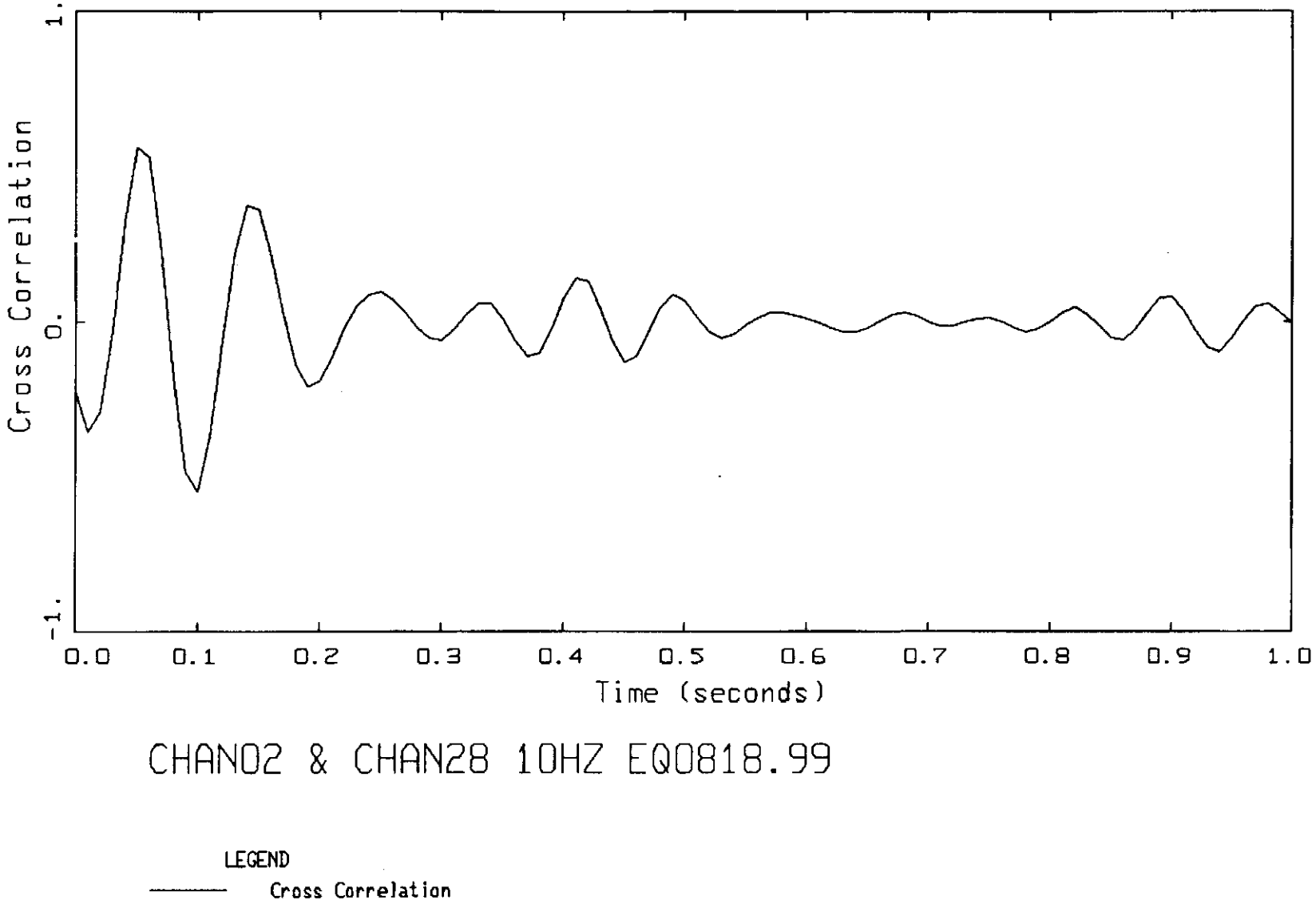

Figure 15. Cross-correlation function at 10 Hz for the vertical surface recording (Channel 2) and the rock recording at 122m (Channel 28) at Treasure Island. The magnitude 5 earthquake occurred on 8/18/99 at an epicentral distance of 29 km.

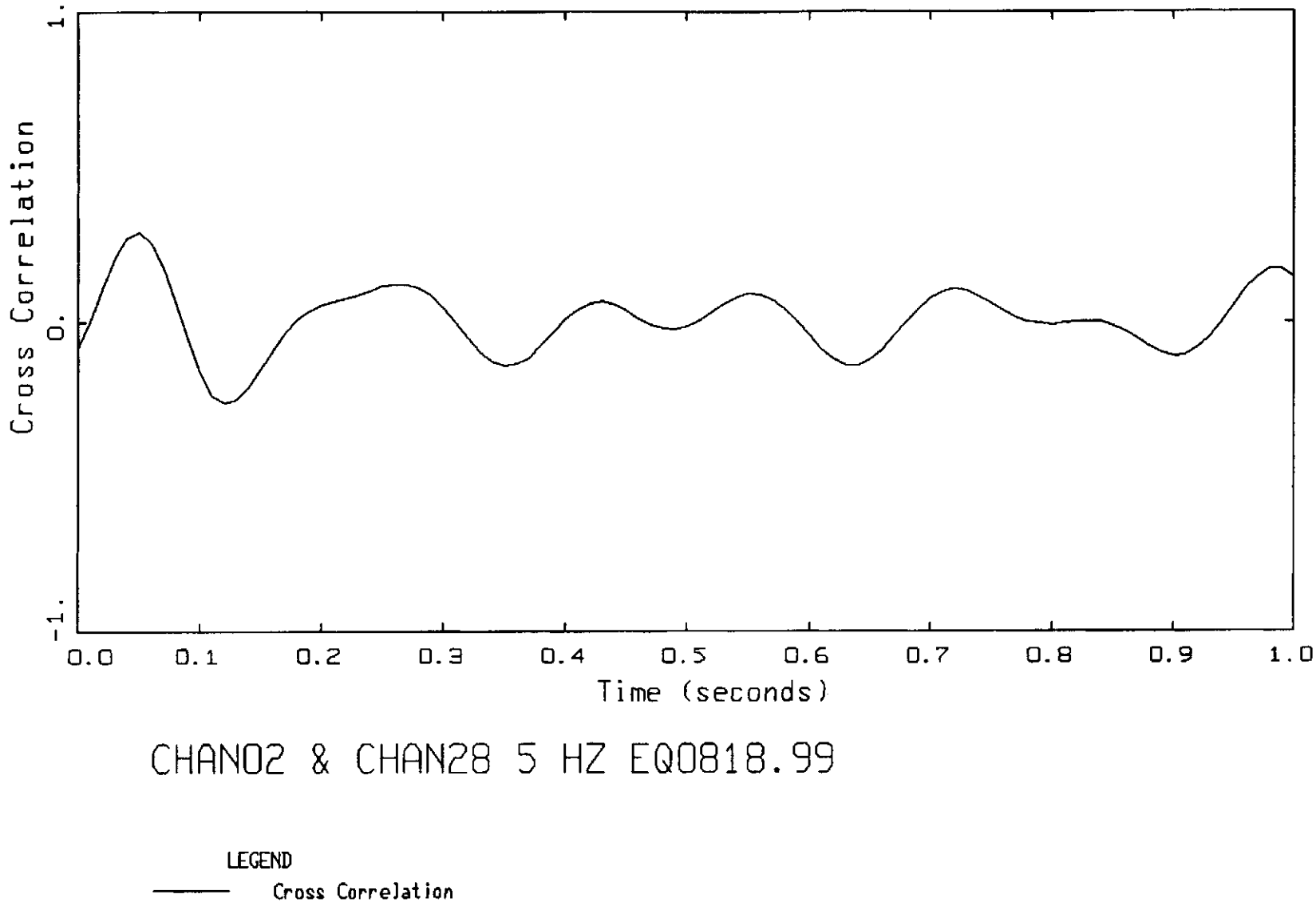

Figure 16. Cross-correlation function at 5 Hz for the vertical surface recording (Channel 2) and the rock recording at 122m (Channel 28) at Treasure Island. The magnitude 5 earthquake occurred on 8/18/99 at an epicentral distance of 29 km.

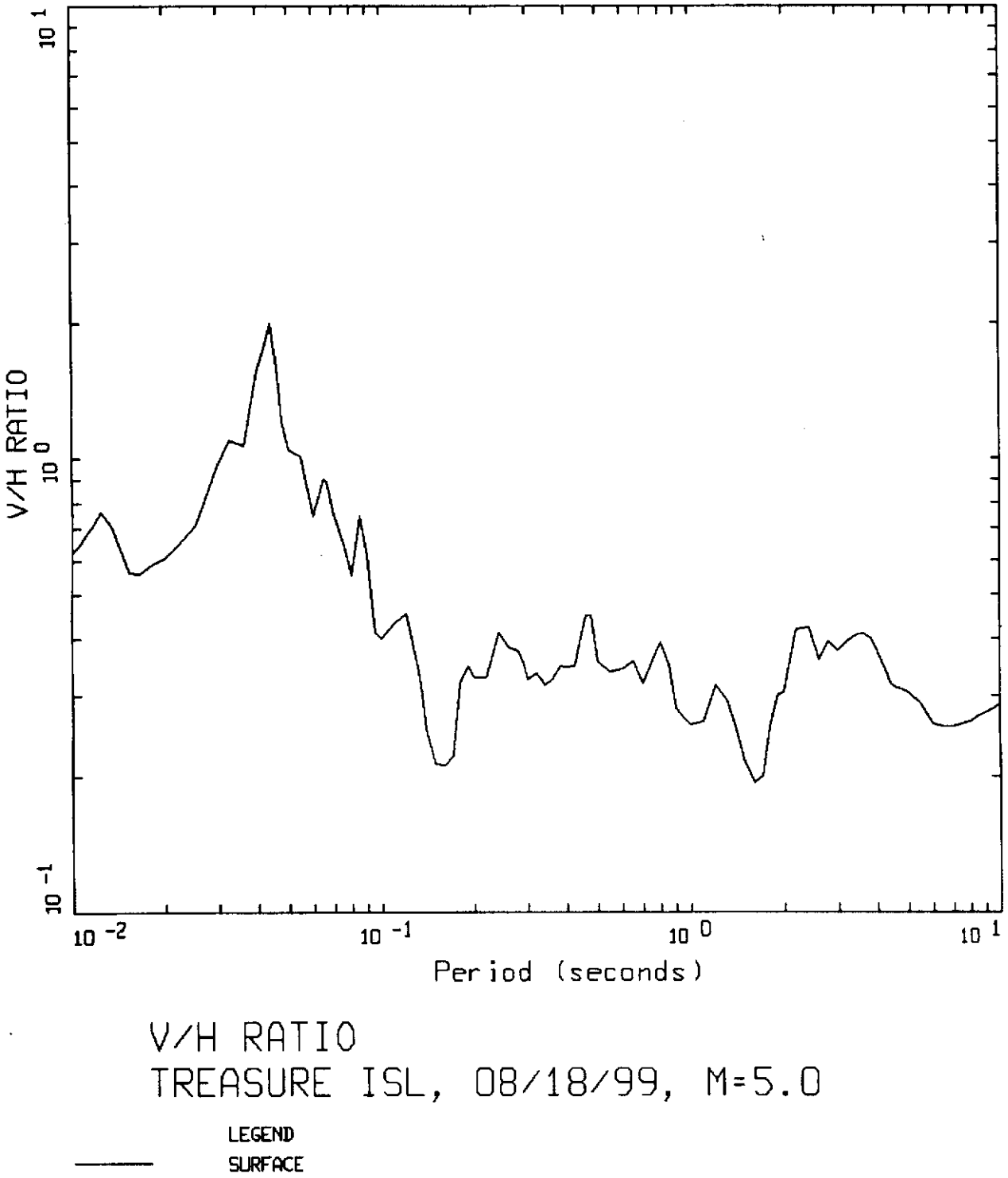

Figure 17. V/H spectral ratio for the surface acceleration time histories at Treasure Island. The magnitude 5 earthquake occurred on 8/18/99 at an epicentral distance of 29 km.

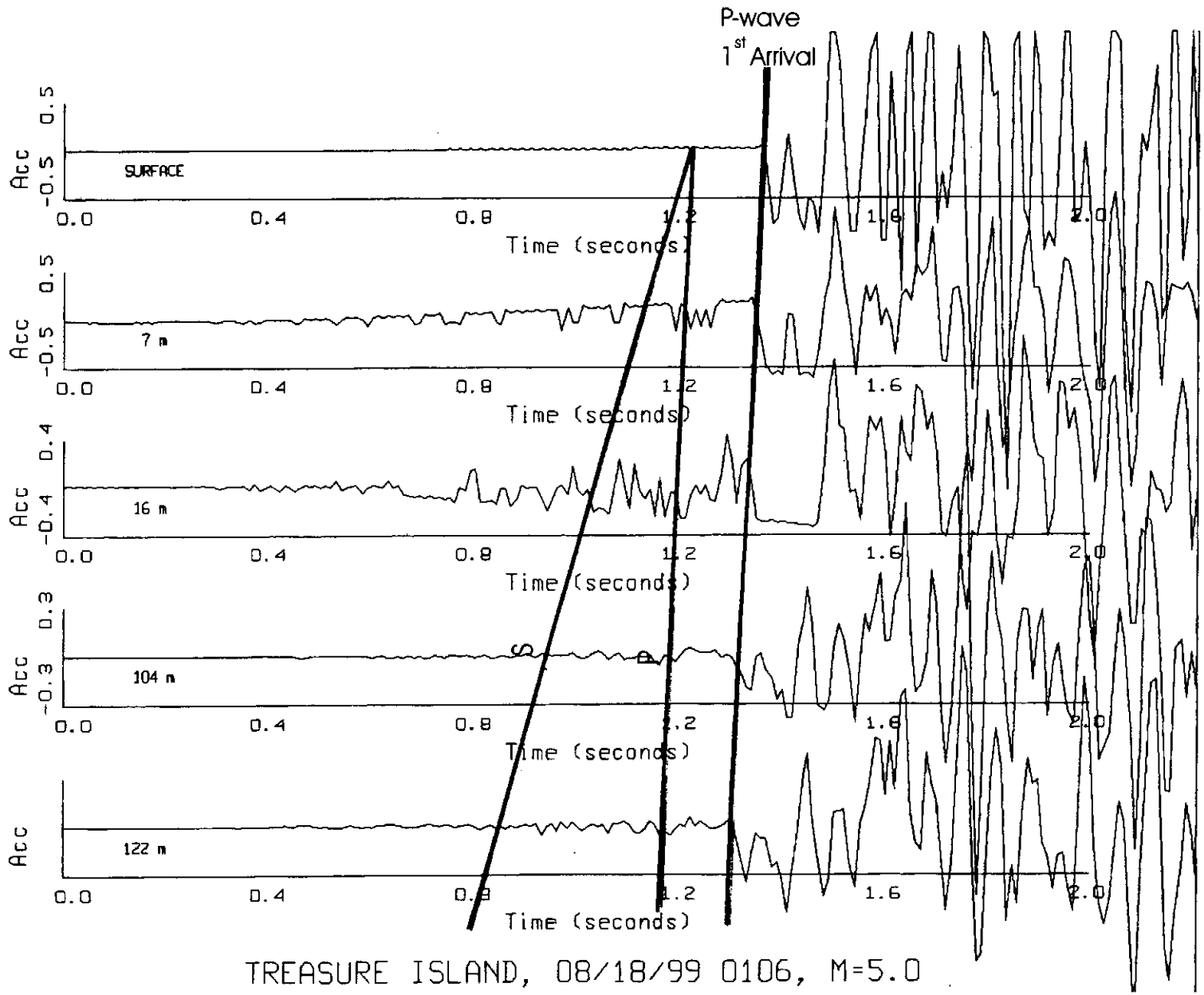

Figure 18. Vertical time histories at the surface, 7m, 16m, 104m, and 122m. The first two seconds of acceleration at Treasure Island are shown. The P-wave first arrival across the array (solid line at first P-wave arrival on the time histories extending from the surface to 122m) propagates at a speed near the average P-wave velocity in the subsurface (solid lines at P-wave and S-wave average profile velocity).

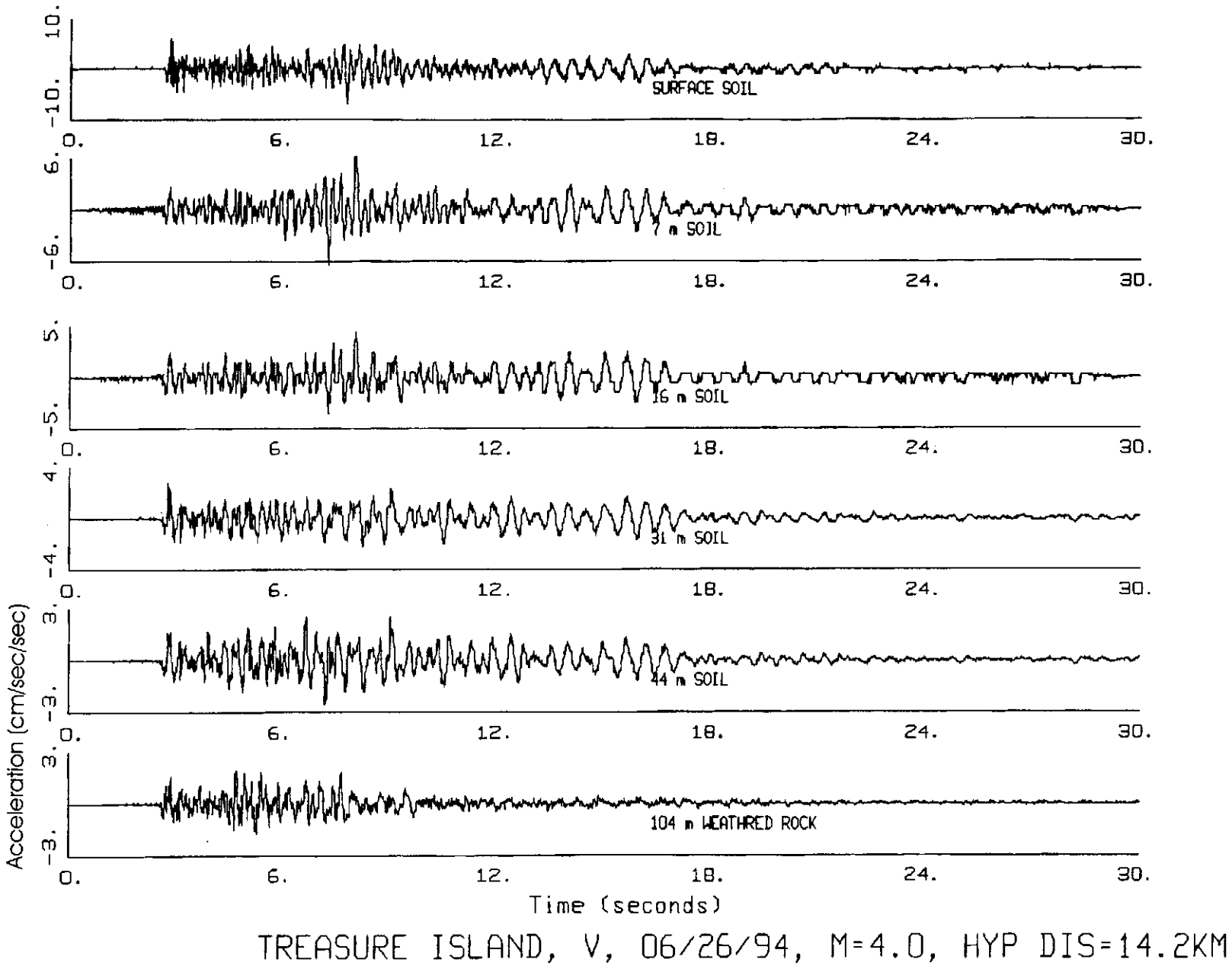

Figure 20. Vertical time histories at the surface, 7m, 16m, 31m, 44m, and 104m The entire acceleration time histories of 30 seconds length at Treasure Island are shown. The magnitude 4.0 earthquake occurred on 6/26/94 at an hypocentral distance of 14.2 km.

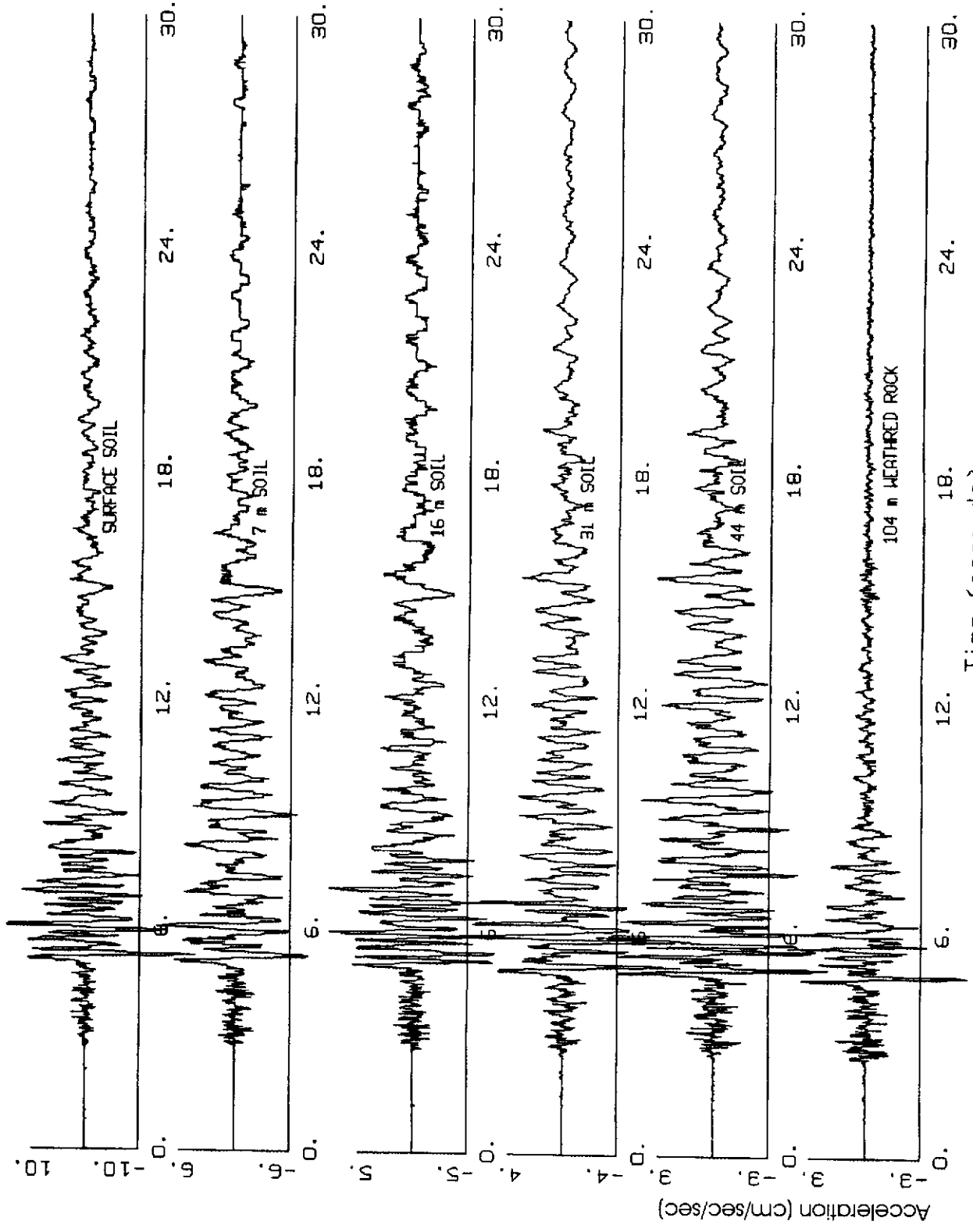

Figure 21. Horizontal time histories at the surface, 7m, 16m, 31m, 44m, and 104m The entire acceleration time histories of 30 seconds length at Treasure Island are shown. The magnitude 4.0 earthquake occurred on 6/26/94 at an hypocentral distance of 14.2 km.

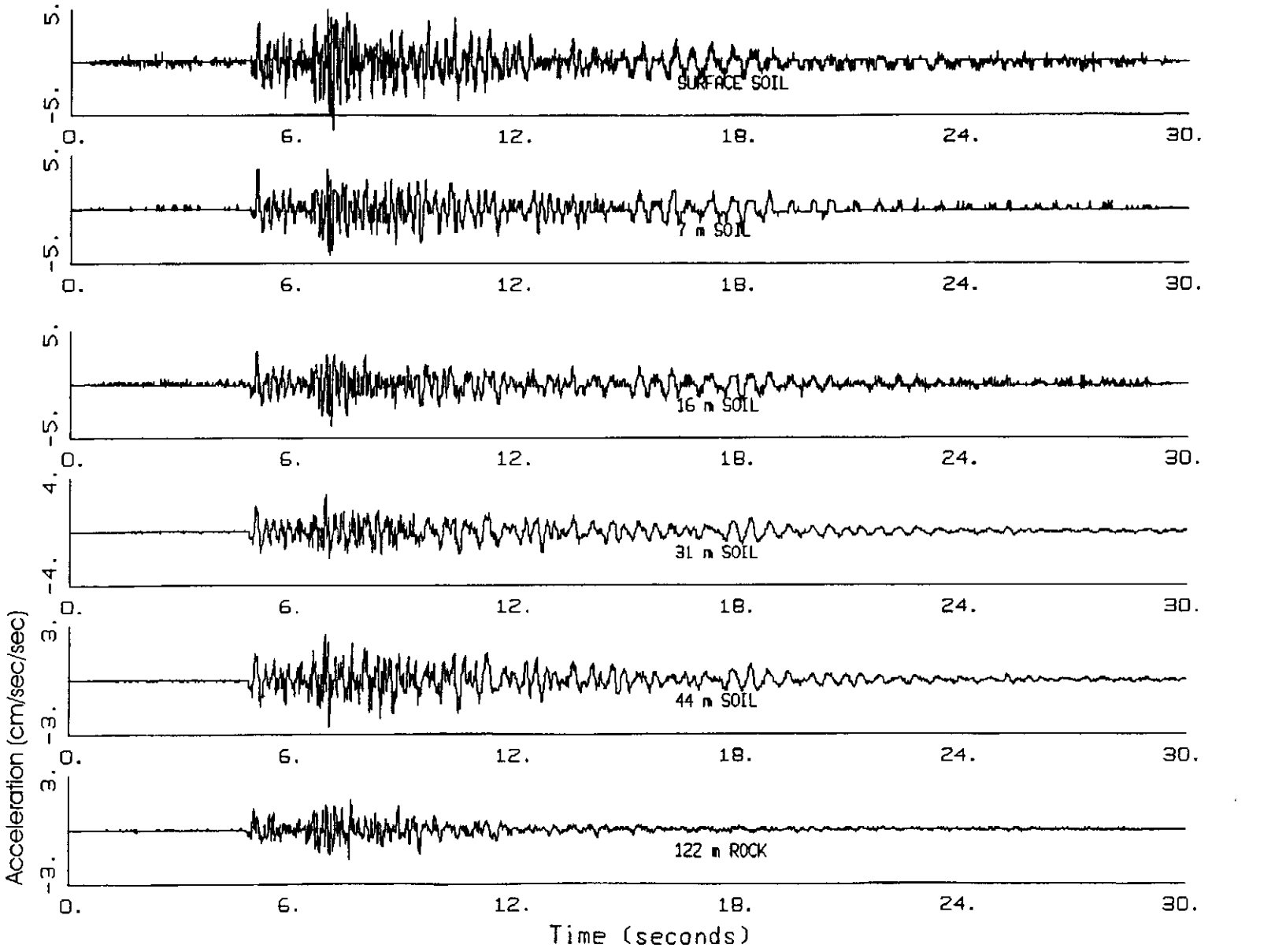

Figure 22. Vertical time histories at the surface, 7m, 16m, 31m, 44m, and 122m The entire acceleration time histories of 30 seconds length at Treasure Island are shown. The magnitude 4.1 earthquake occurred on 12/4/98 at an hypocentral distance of 14.7 km.

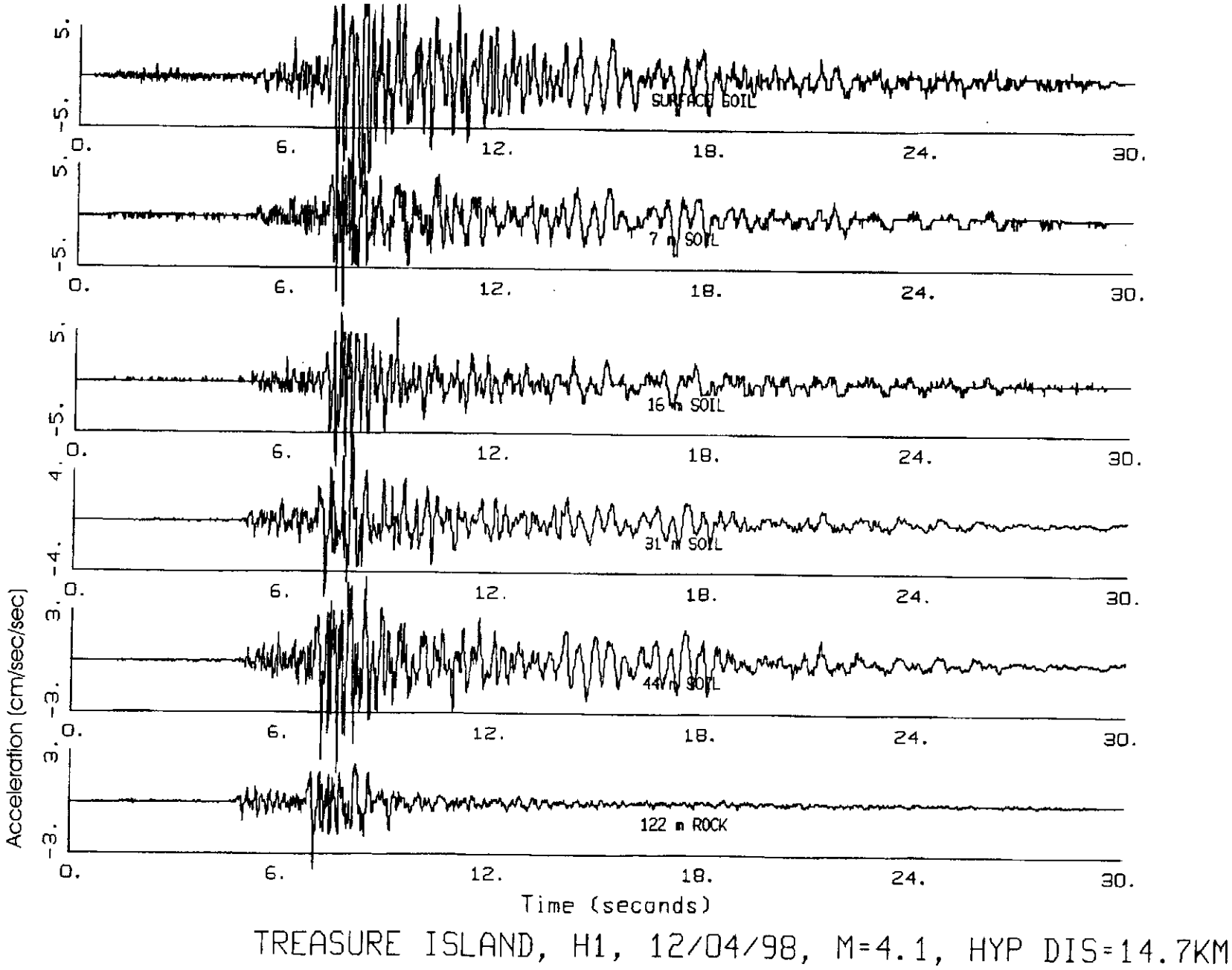

Figure 23. Horizontal time histories at the surface, 7m, 16m, 31m, 44m, and 122m The entire acceleration time histories of 30 seconds length at Treasure Island are shown. The magnitude 4.1 earthquake occurred on 12/4/98 at an hypocentral distance of 14.7 km.

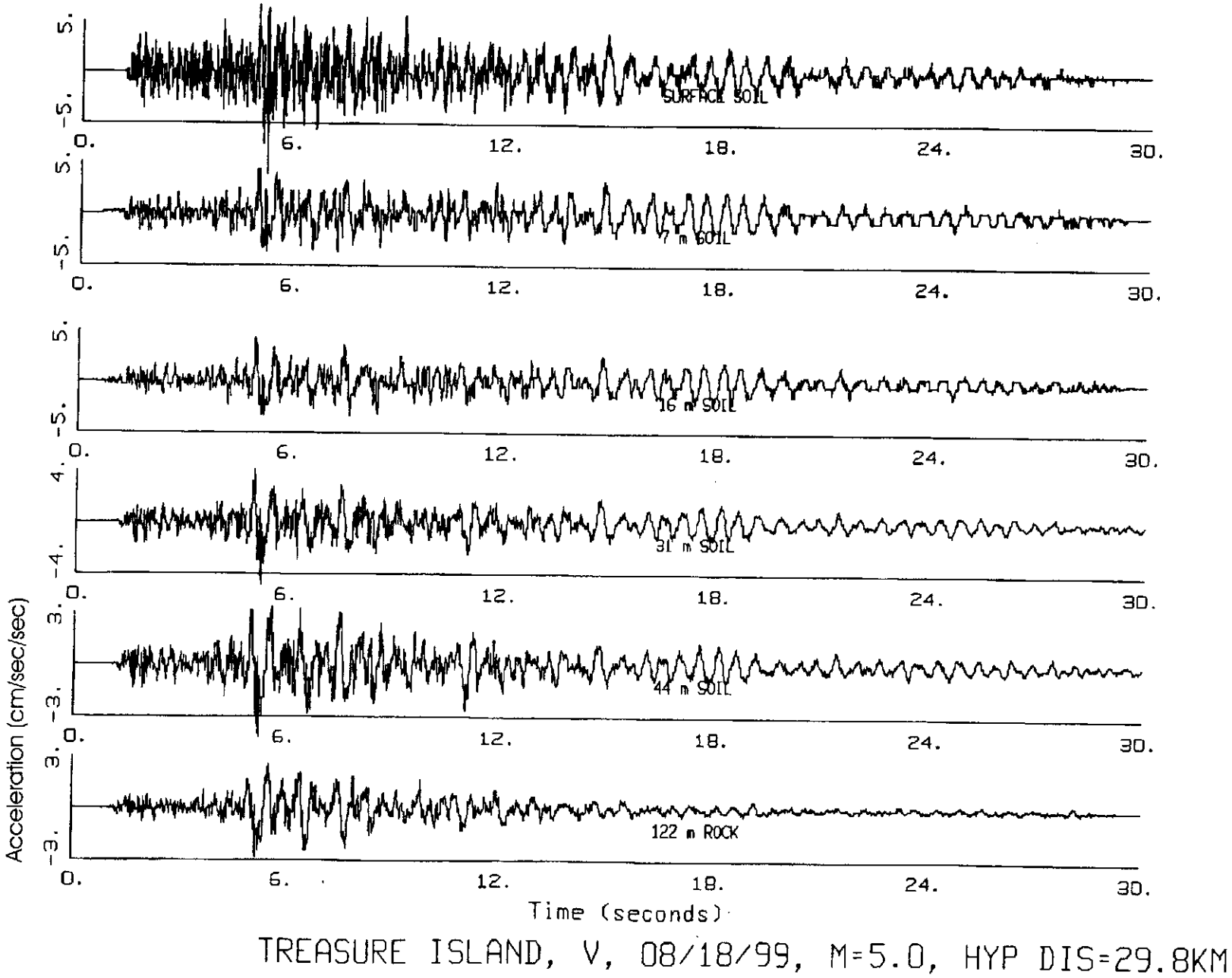

Figure 24. Vertical time histories at the surface, 7m, 16m, 31m, 44m, and 122m The entire acceleration time histories of 30 seconds length at Treasure Island are shown. The magnitude 5.0 earthquake occurred on 8/18/99 at an hypocentral distance of 29.8 km.

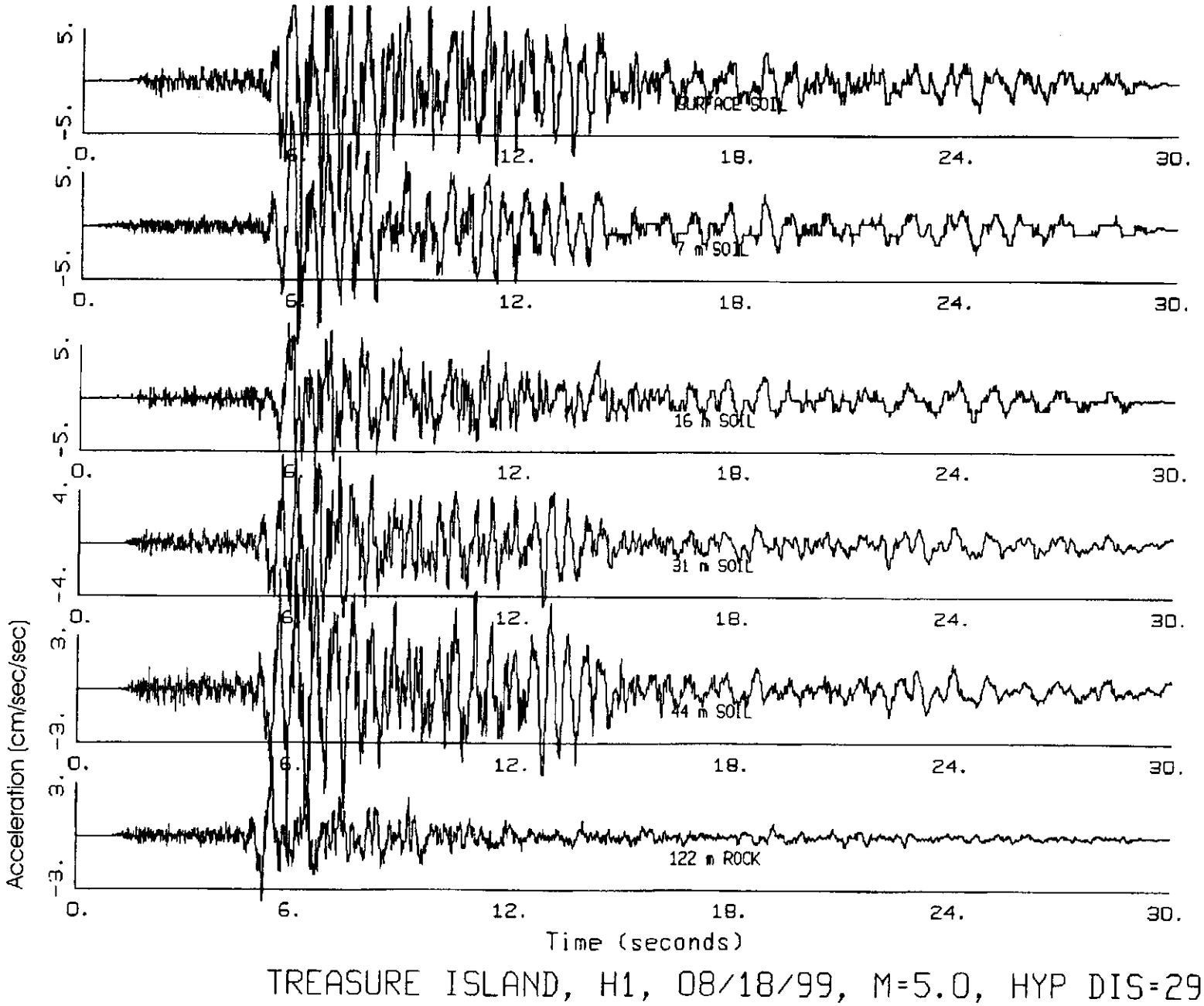

Figure 25. Horizontal time histories at the surface, 7m, 16m, 31m, 44m, and 122m The entire acceleration time histories of 30 seconds length at Treasure Island are shown. The magnitude 5.0 earthquake occurred on 8/18/99 at an hypocentral distance of 29.8 km.

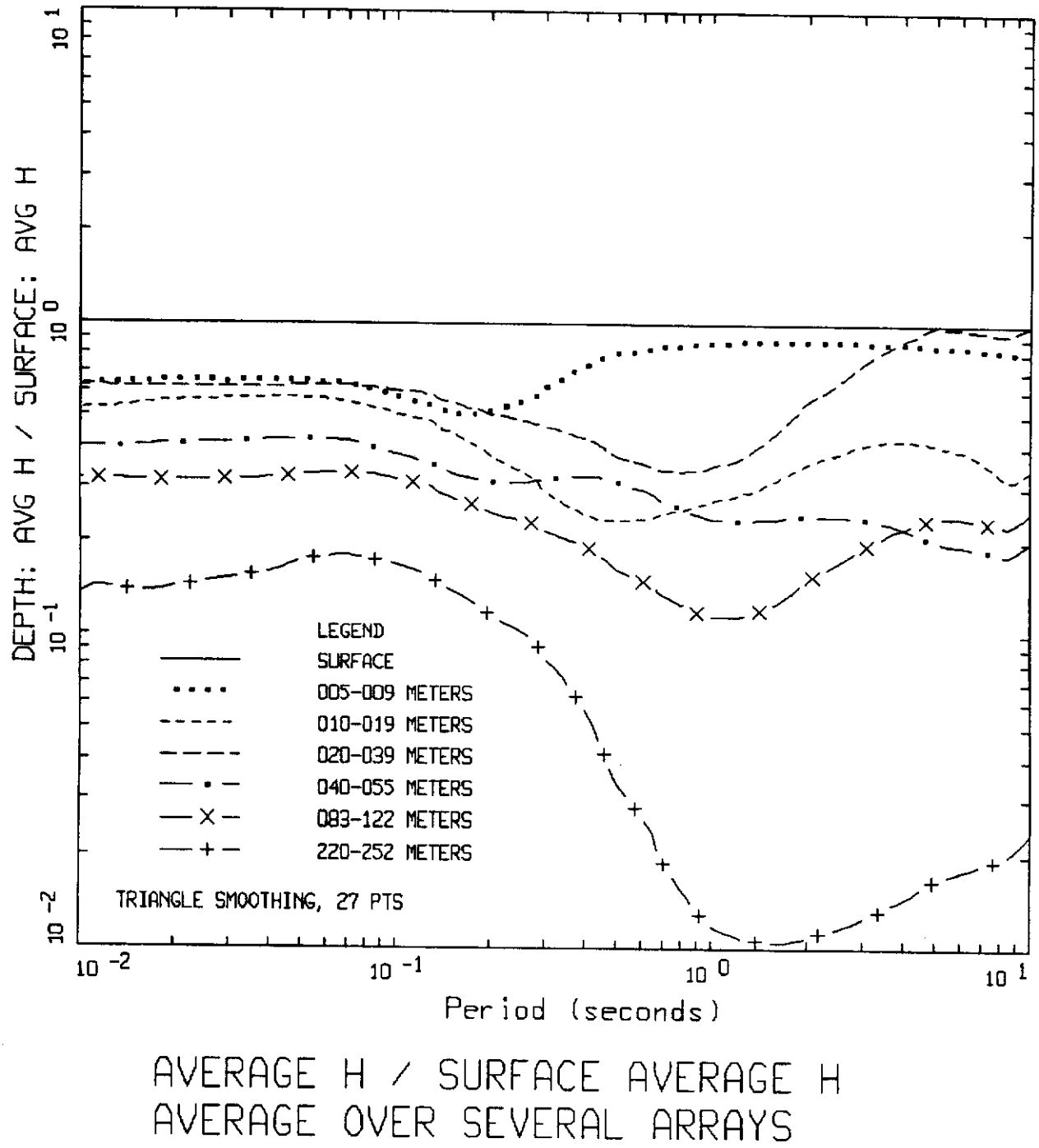

Figure 26. Normalized average horizontal response spectra (5% damping). The average spectra are normalized by the average horizontal surface spectrum. The surface ratio is shown on the plots as the solid line at unity. The ratio is shown for six depth ranges. The ratio is an average taken over several arrays.

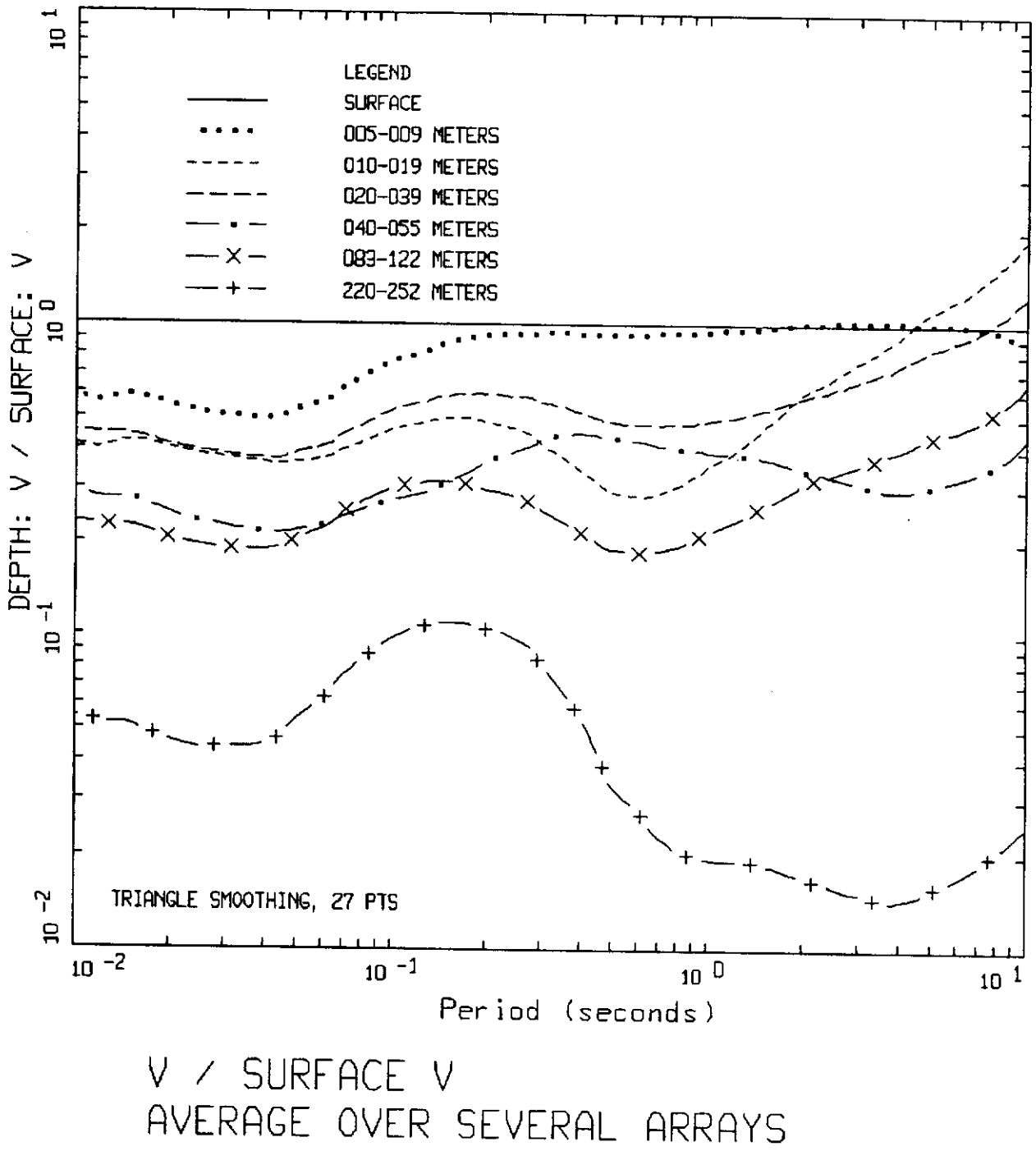

Figure 27. Normalized vertical response spectra (5% damping). The vertical spectra are normalized by the vertical surface spectrum. The surface ratio is shown on the plots as the solid line at unity. The ratio is shown for six depth ranges. The ratio is an average taken over several arrays.

APPENDIX A

VERTICAL ARRAY VELOCITY PROFILES

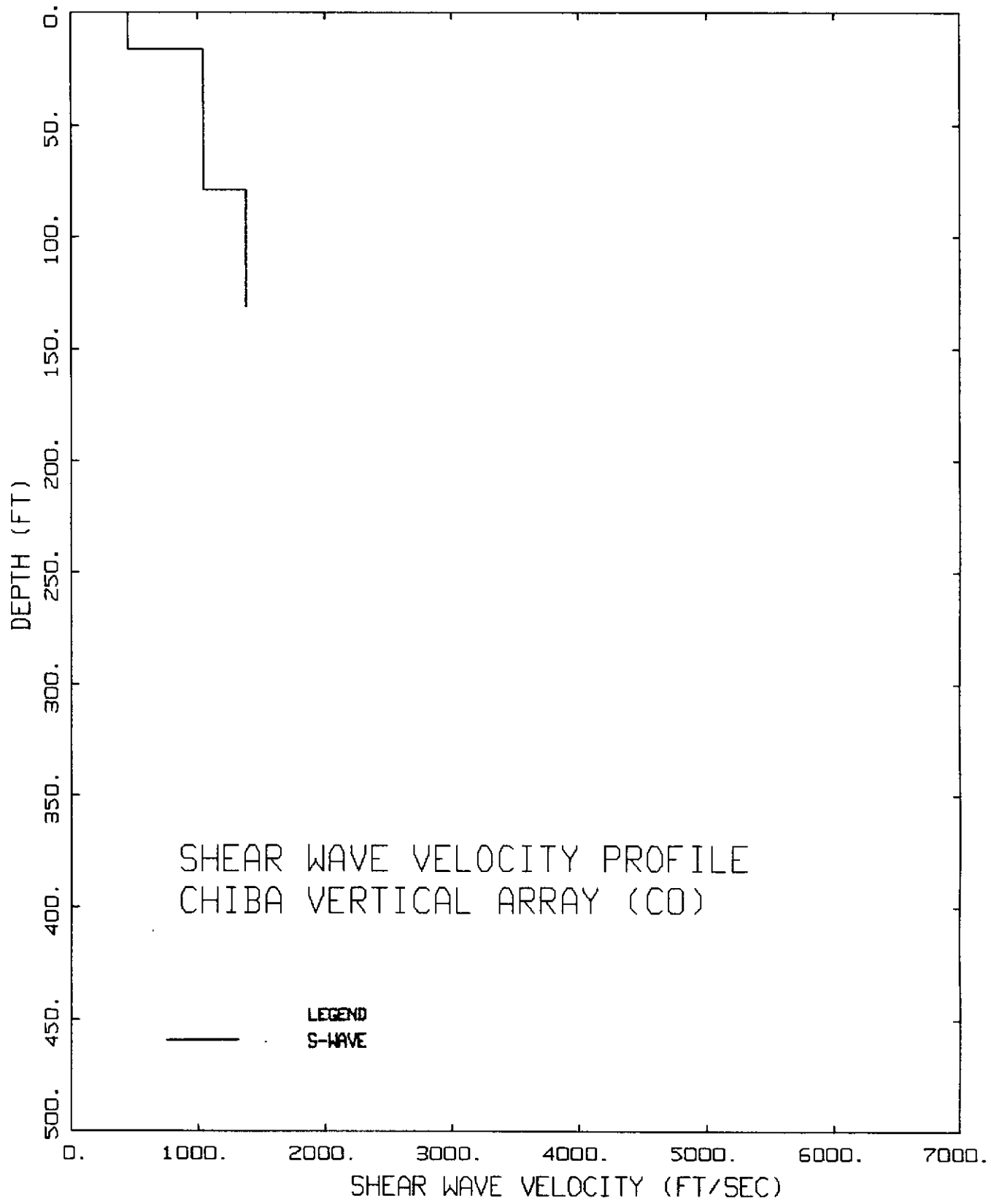

Figure A-1. S-wave velocity profile for Chiba, Japan.

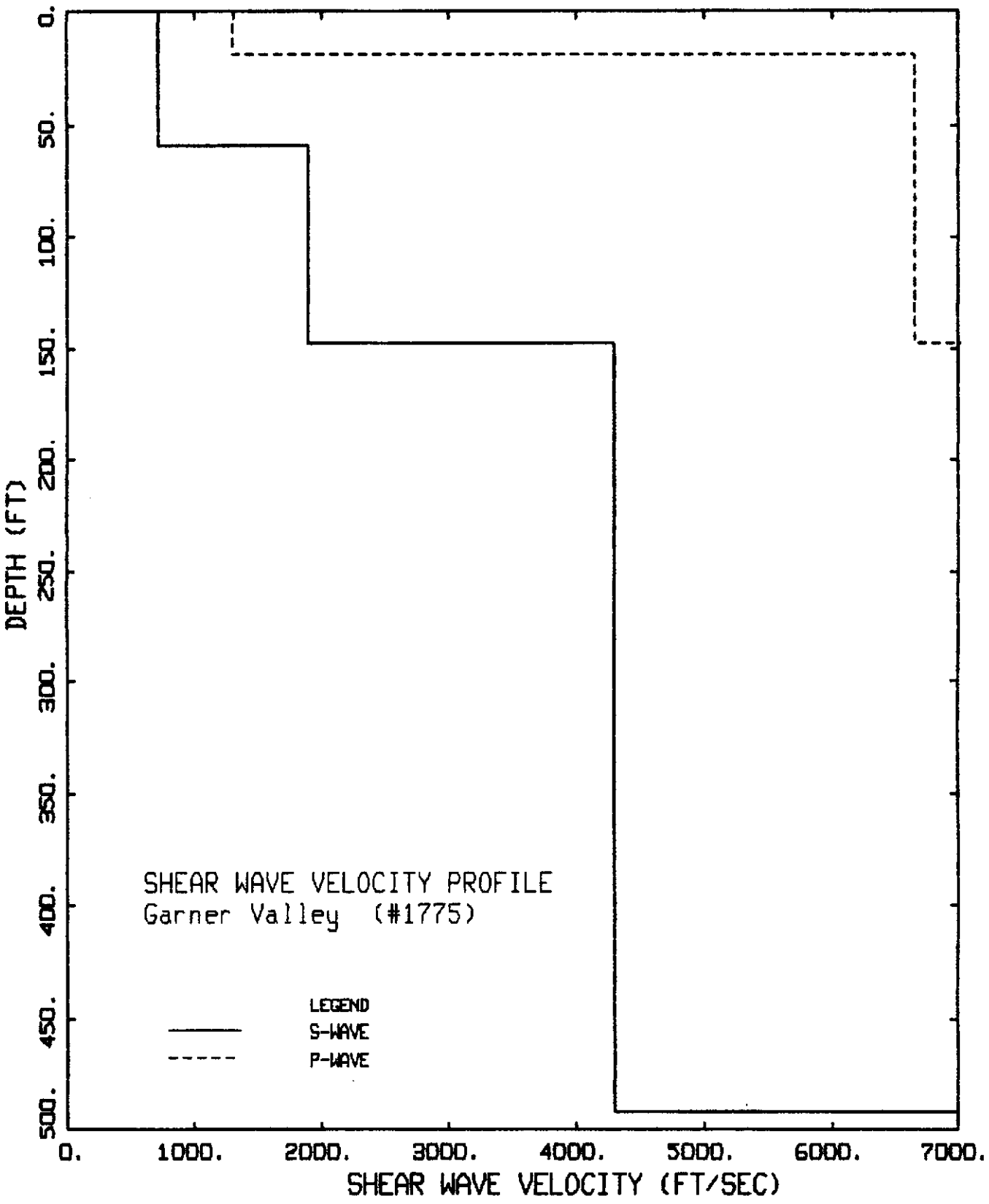

Figure A-2. S-wave and P-wave velocity profiles for Garner Valley, California.

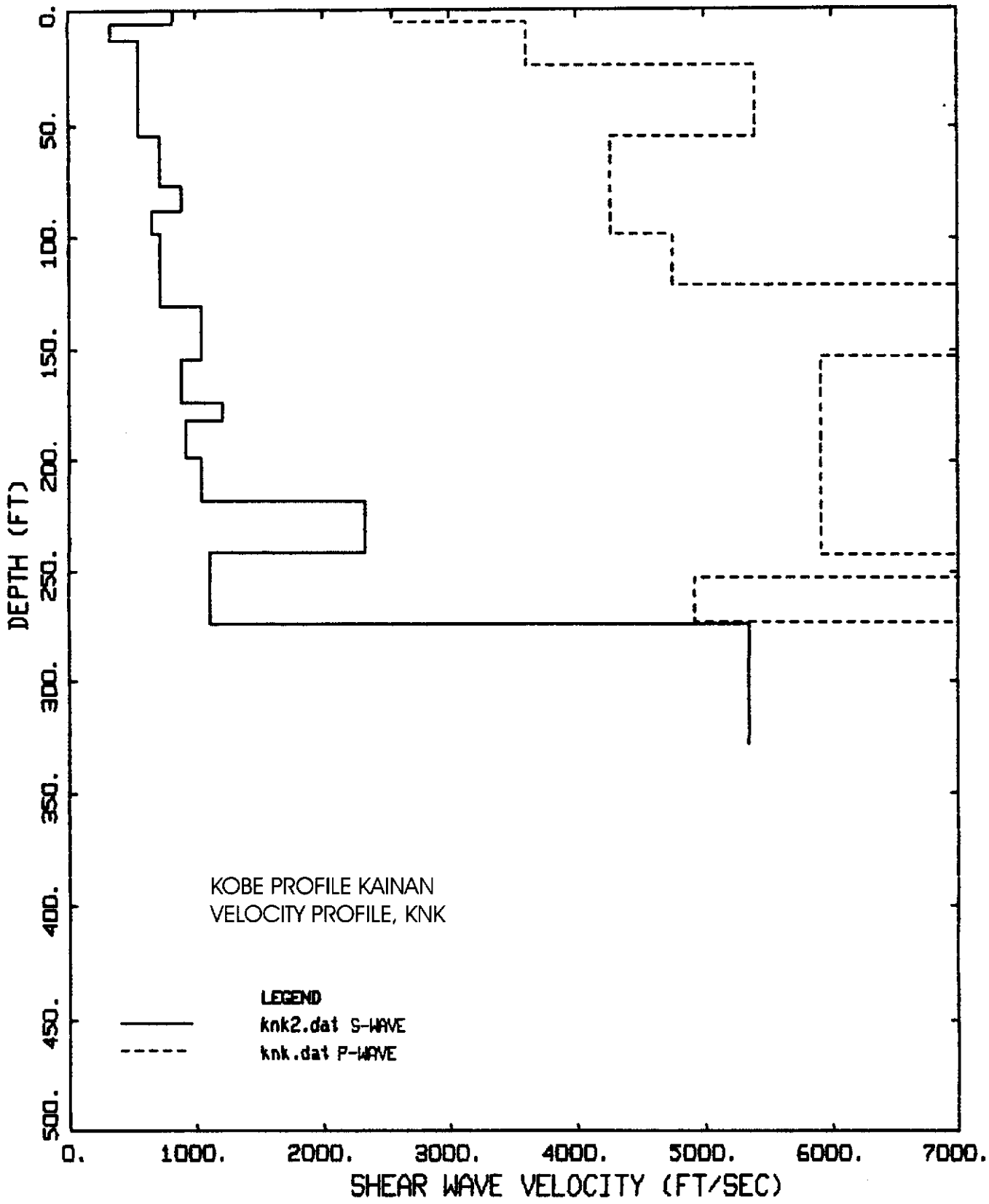

Figure A-3. S-wave and P-wave velocity profiles for Kainan, Japan.

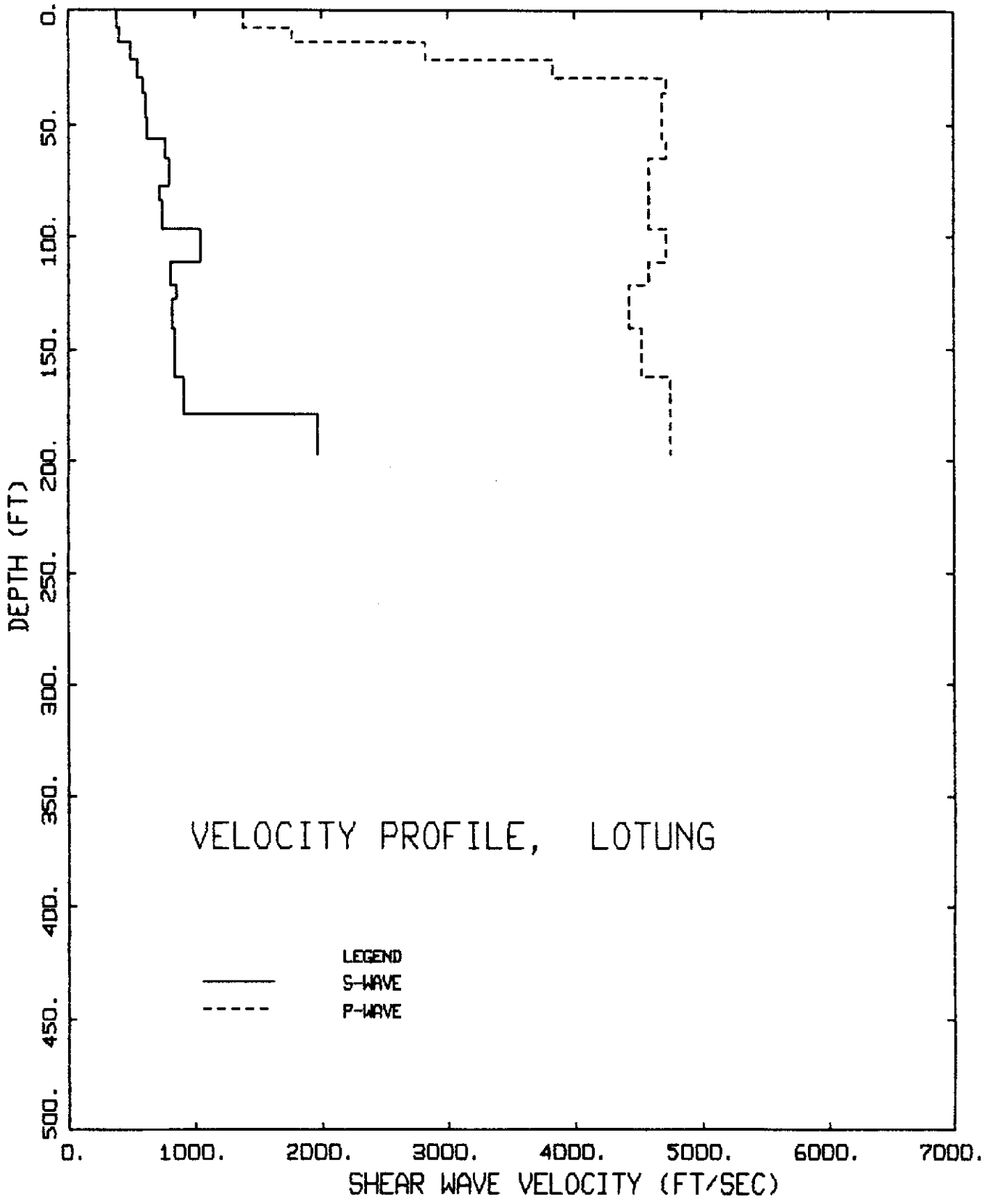

Figure A-4. S-wave and P-wave velocity profiles for LSST-Lotung, Taiwan.

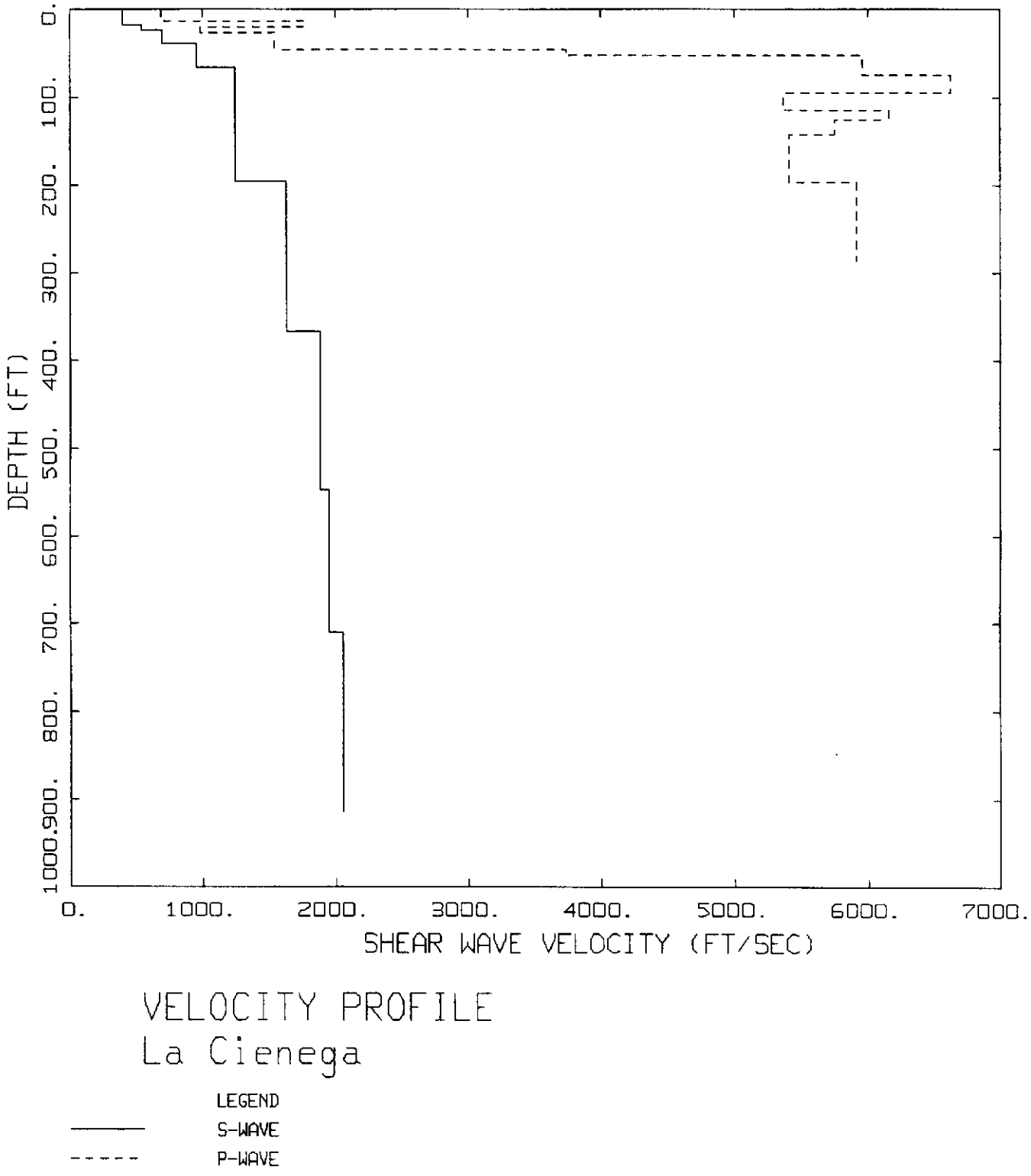

Figure A-5. S-wave and P-wave velocity profiles for La Cienega, California.

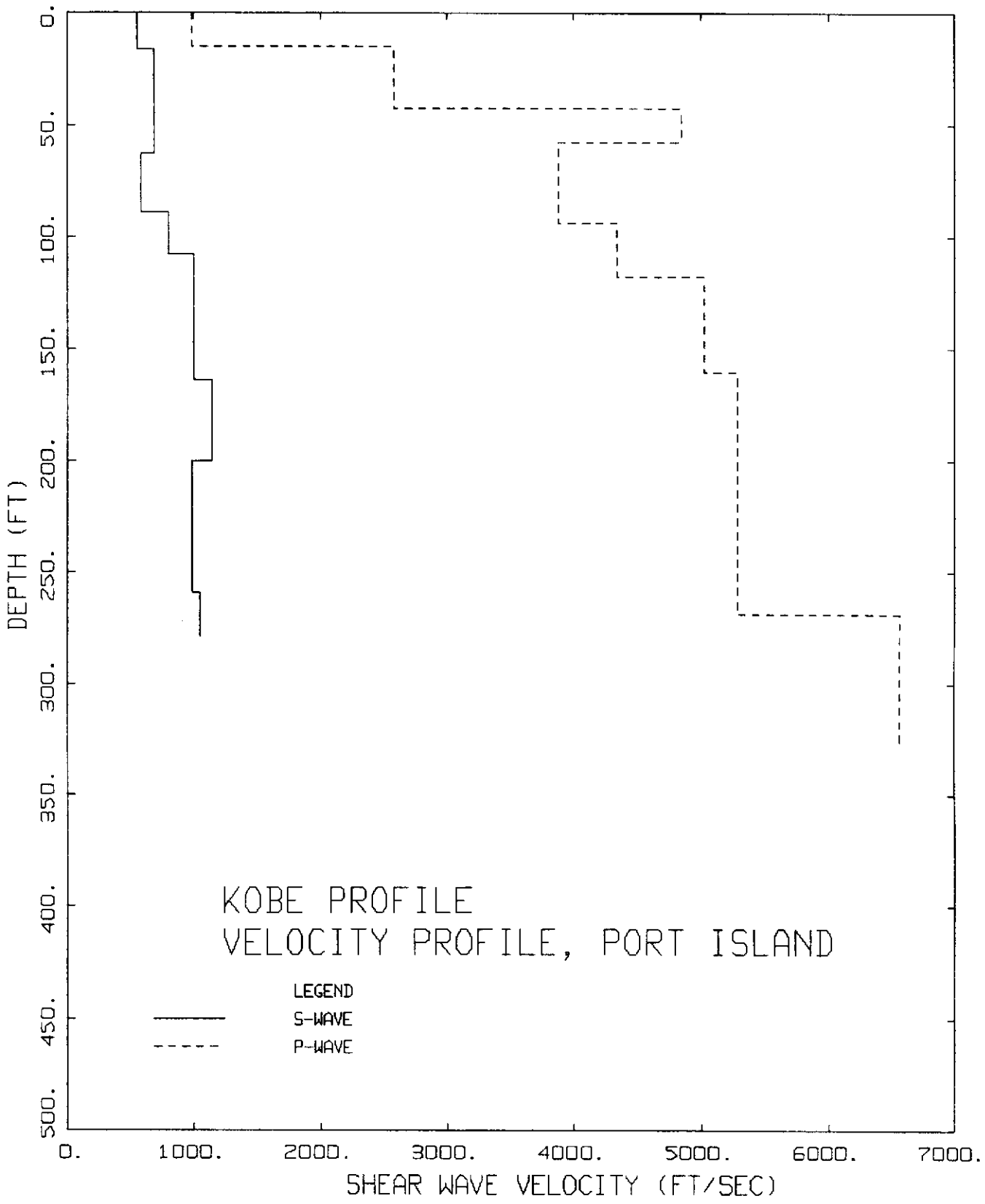

Figure A-6. S-wave and P-wave velocity profiles for Port Island, Japan.

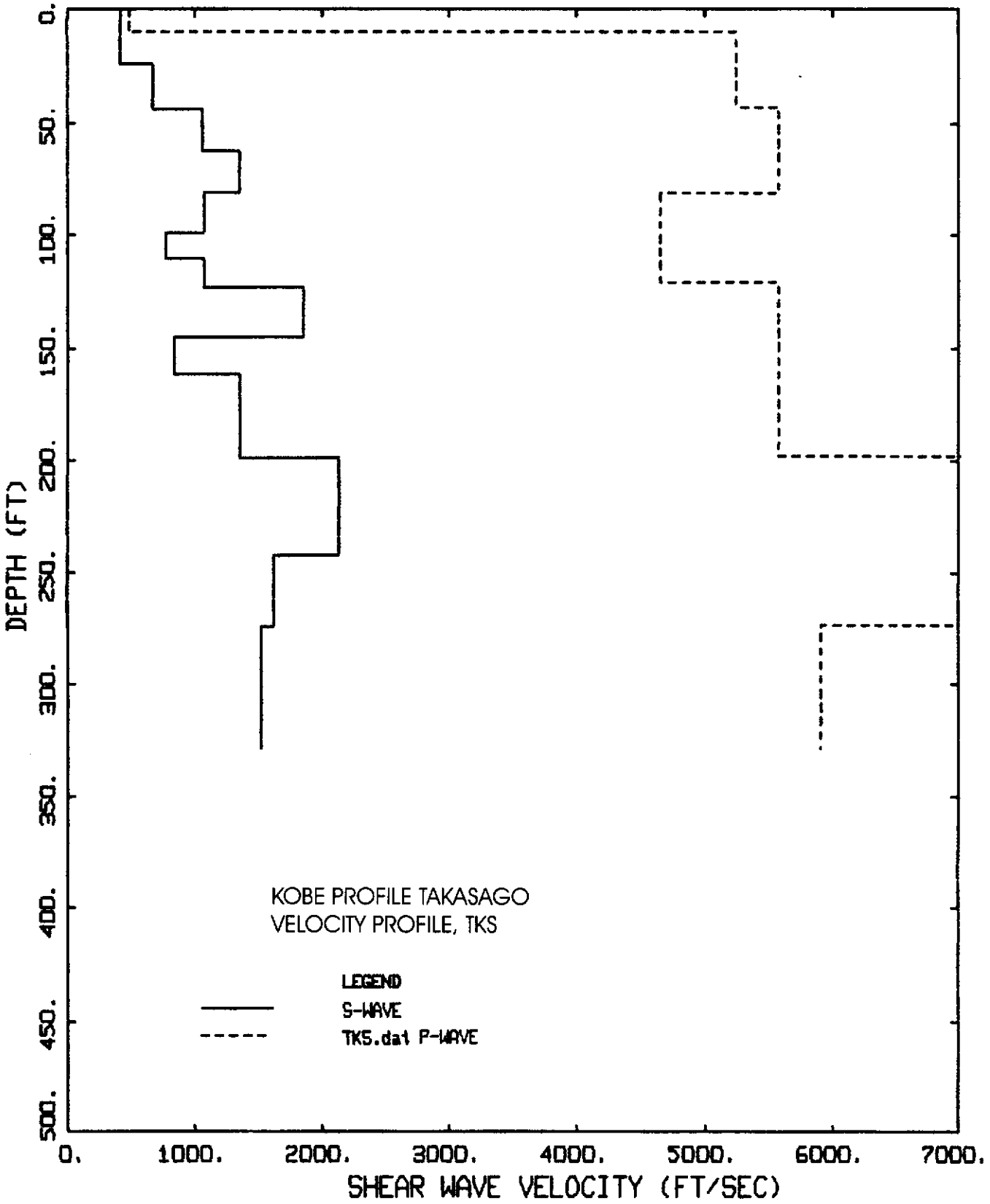

Figure A-7. S-wave and P-wave velocity profiles for Takasago, Japan.

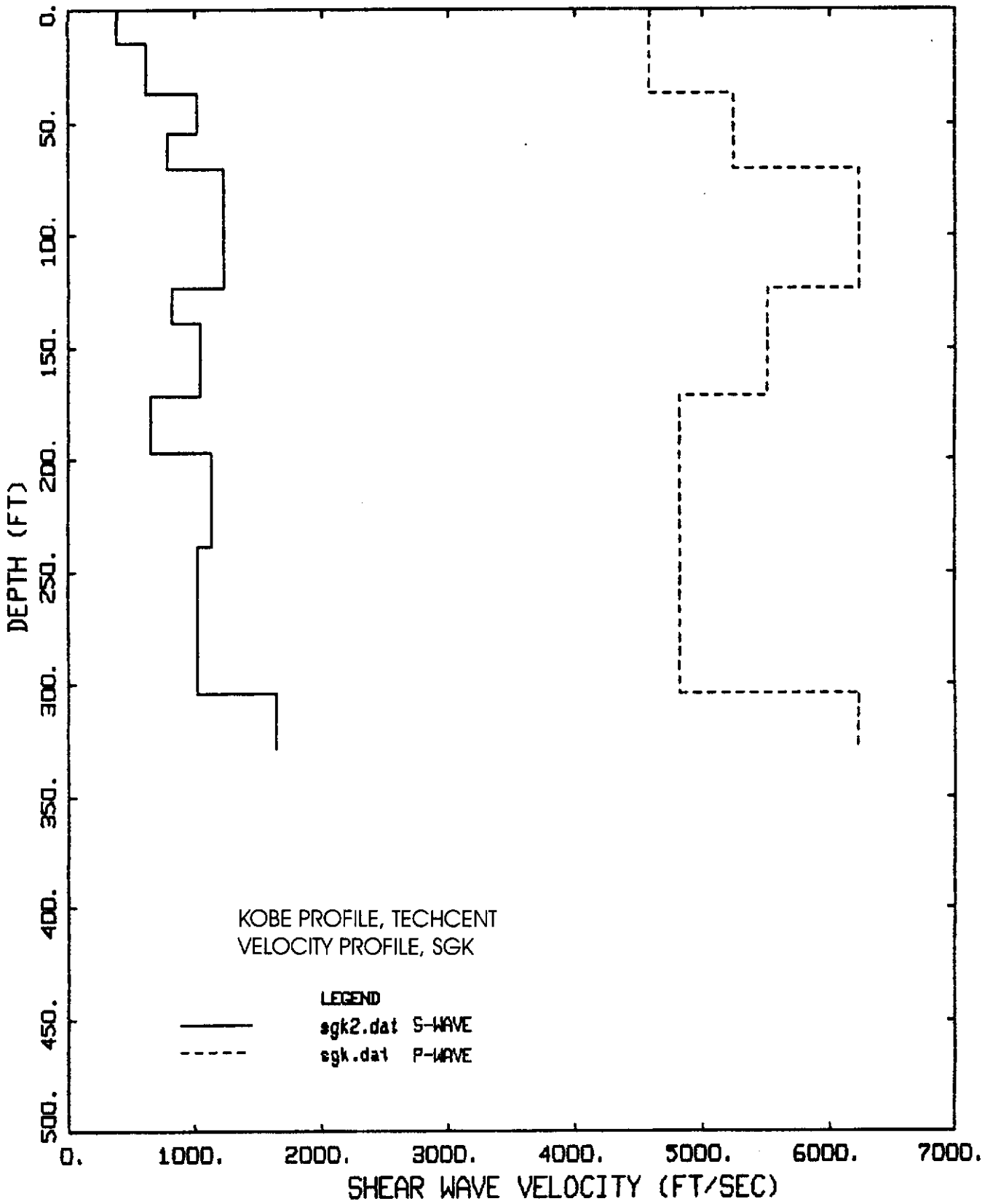

Figure A-8. S-wave and P-wave velocity profiles for Techcent, Japan.

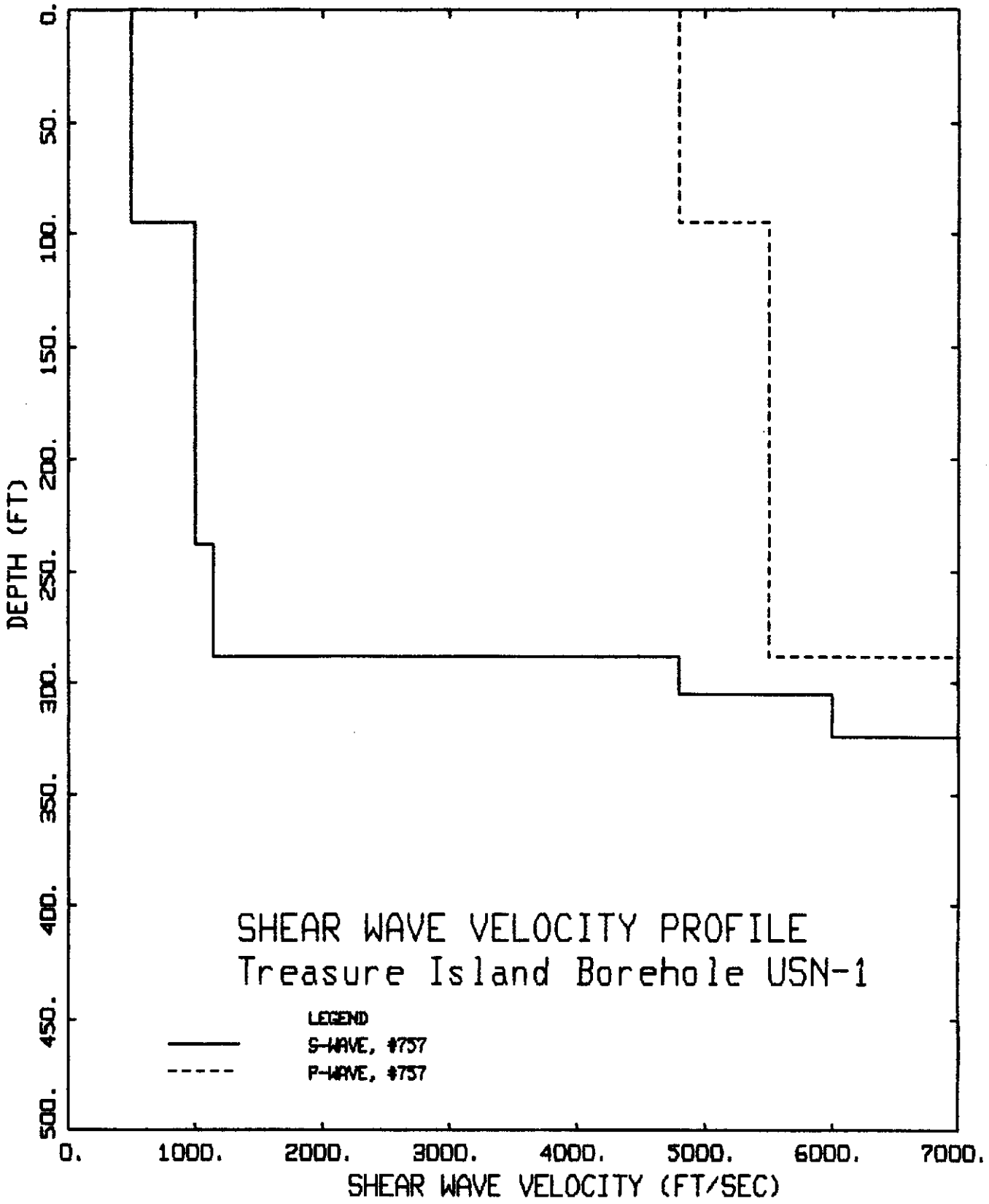

Figure A-9. S-wave and P-wave velocity profiles for Treasure Island, California.

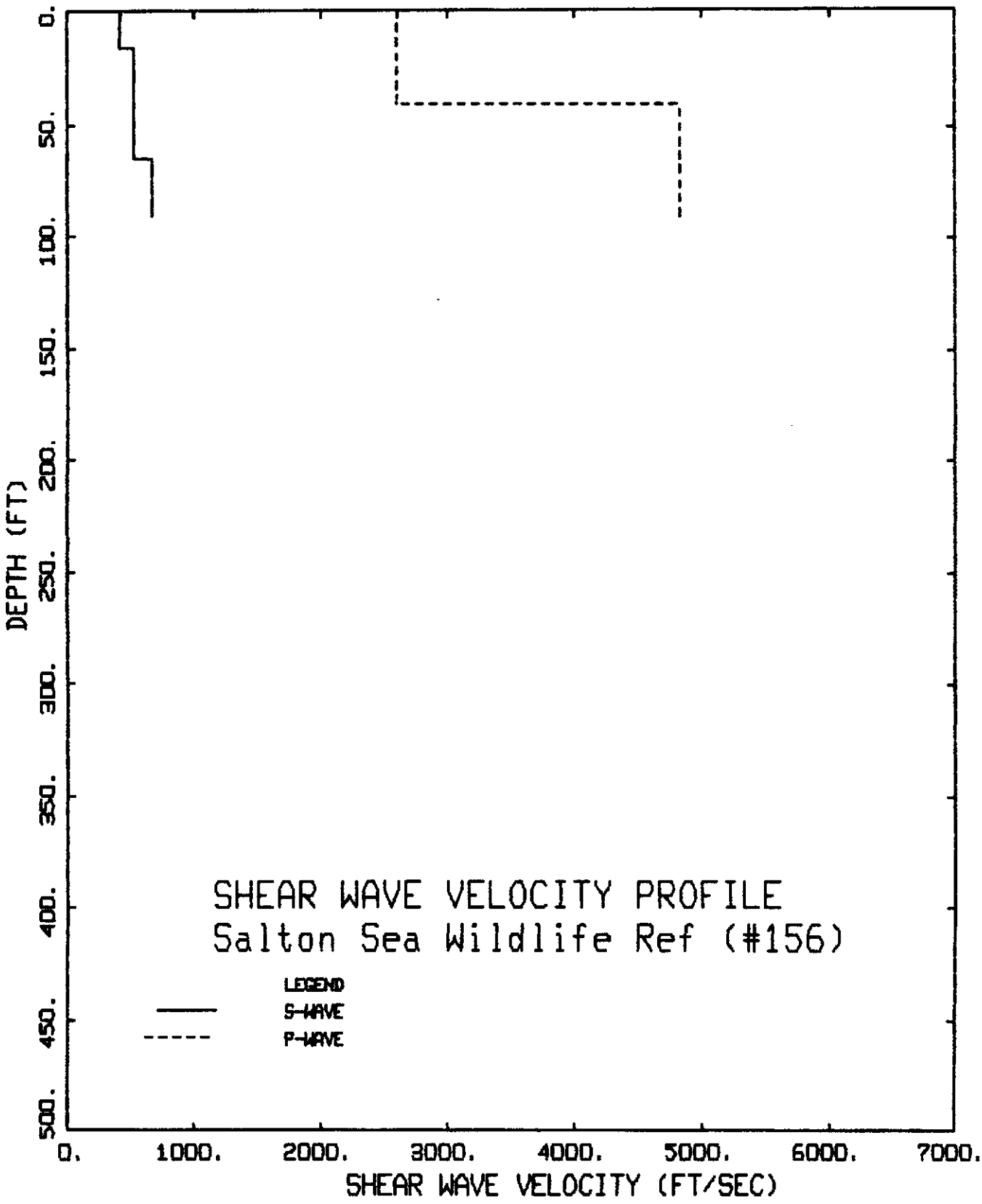

Figure A-10. S-wave and P-wave velocity profiles for Liquefaction Island, California.

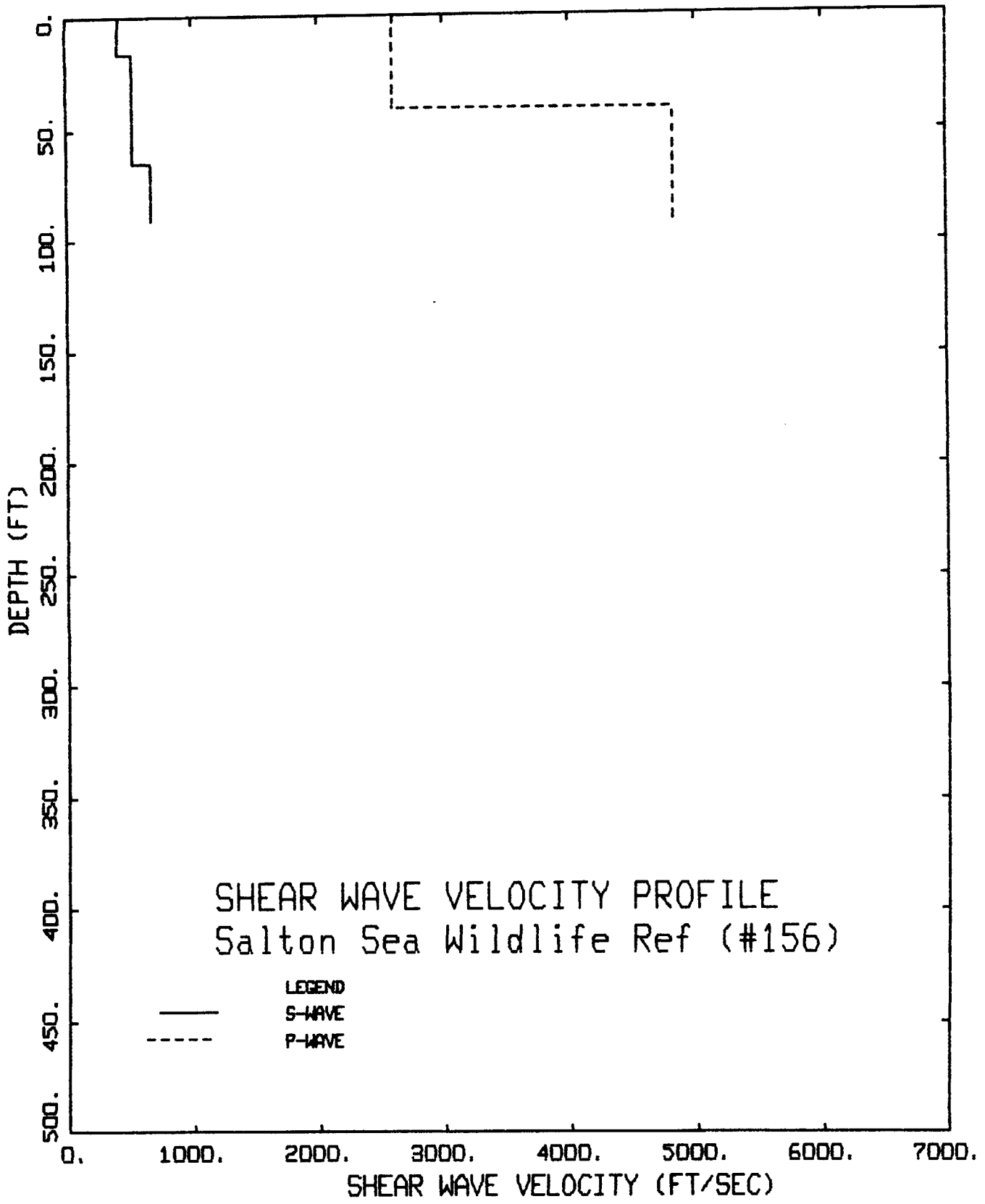

Figure A-10. S-wave and P-wave velocity profiles for Liquefaction Island, California.